

Processing and Characterization of Membranes
Based on Cellulose Nanocrystals for
Water Purification

Zoheb Karim

**Processing and characterization of membranes based on
cellulose nanocrystals for water purification**

Zoheb Karim

Luleå

2014-11-28

Division of Materials Science, Department of Engineering Sciences and
Mathematics

AND

Division of Sustainable Process Engineering, Department of Civil,
Environmental and Natural Resources Engineering,
Luleå University of Technology

Printed by Luleå University of Technology, Graphic Production 2014

ISSN 1402-1757

ISBN 978-91-7583-049-0 (print)

ISBN 978-91-7583-050-6 (pdf)

Luleå 2014

www.ltu.se

Abstract

Membrane technology is being extensively used in water purification as an energy efficient and low cost process. Nanostructured (NSM) and nanoenabled (NEM) membranes are favored in this context as nanoscaled entities are expected to provide high surface area, high mechanical properties and versatile surface chemistry as well as provide better control on the pore size and distribution, flux and selectivity of the membrane. Biobased nanoparticles as nanocrystals are expected to have a significant advantage in this context. Thus, the main aim of this work was to explore the use of cellulose nanocrystals as functional entities for the fabrication of nanoenabled composite membranes and apply these fabricated membranes for the removal of dyes and metal ions from polluted water.

The first study deals with the isolation of cellulose nanocrystals (CNC_{BE}) from wood using the bioethanol pilot scale setup. Cellulose was prepared from wood by diluted acid treatment in the bioethanol plant followed by dewaxing and bleaching. The cellulose was converted into cellulose nanocrystals by mechanical grinding using lab scale homogenizer. The isolated nanoparticles had a diameter of 5-15 nm and formed a thick gel at 2 wt%. X-ray photoelectron spectroscopy illustrated the presence of O=C-O surface functional groups, directly related to the negative zeta-potential values. Fabricated films of CNC_{BE} denoted good mechanical properties, optical properties and cytocompatibility. Thus, a new isolation route that can be followed to produce nanocrystals in large quantities (600 g/ day) has been developed.

In a second study, fully biobased nanocomposite membranes of cellulose nanocrystals and chitosan have been fabricated by freeze-drying and crosslinking with gluteraldehyde in vapor phase. The chitosan bound the CNC_{SL} in a stable and nanoporous membrane network with thickness of 250-270 μm . Homogenous dispersion of CNC_{SL} within chitosan matrix was reported based on scanning electron microscopy (SEM). The Brunauer Emmett and Teller (BET) studies showed a decrease in surface area (3.1 to 2.9 m^2/g) and average pore size (17 to 13 nm) after crosslinking. The mechanical performance of composite membranes was low, being 0.98 ± 0.4 and 1.1 ± 0.3 MPa of tensile strength for uncross-linked and cross-linked membranes, respectively. In spite of low water flux ($64 \text{ L m}^{-2} \text{ h}^{-1}$), the composite membranes successfully removed 98%, 84% and 70% respectively of positively

charged dyes like Victoria Blue 2B, Methyl Violet 2B and Rhodamine 6G, from a model wastewater after a contact time of 24 h.

In the third study layered membranes containing a highly porous support layer and a dense functional layer has been fabricated following a filtration and hot pressing method. Microsized cellulose fibers from sludge bioresidues was used as the support layer to provide mechanical stability and allow water flow without any hindrance. A nanocomposite system of nanocrystals (CNC_{SL} , CNC_{BE} and PCNC_{SL}) with gelatin as matrix was used as the functional layer. Bubble point measurement confirmed the membrane pore sizes (5-6 μm), in microfiltration range, which resulted in high water permeability $< 4000 \text{ Lh}^{-1}\text{m}^{-2}$ at 1.5 bars. Efficient removal of Ag^+ , Cu^{2+} and Fe^{3+} from industrial wastewater was achieved using these membranes. The removal of metal ions was expected to be driven by the electrostatic attraction between negatively charged nanocellulose and the positively charged metal ions.

The work has demonstrated that highly efficient water treatment membranes can be fabricated from nanocellulose via tailoring their ability to interact and selectively adsorb heavy metal ions and dyes.

List of appended papers

Paper A

Aji P. Mathew, Kristiina Oksman, Zoheb Karim, Peng Liu, Saad Ahmed Khan, Narges Naseri, Process scale up and characterization of wood cellulose nanocrystals hydrolysed using bioethanol pilot plant. *Industrial Crop and Products* 58 (2014) 212-219.

Paper B

Zoheb Karim, Aji P. Mathew, Mattias Grahn, Johanne Mouzon, Kristina Oksman, Nanoporous membranes with cellulose nanocrystals as functional entity in chitosan: Removal of dyes from water. *Carbohydrate Polymers* 112 (2014) 668-676.

Paper C

Zoheb Karim, Aji P. Mathew, Mojca Bozic, Vanja Kokol, Jiang Wei, Mattias Grahn, Kristiina Oksman, High flux affinity membranes based on cellulose nanocomposite for removal of heavy metal ions from industrial effluent. *Submitted to Environmental Science and Technology*.

Other related paper

Paper D

Zoheb Karim, Simon Claudpierre, Kristiina Oksman, Aji P. Mathew, Nanocellulose based functional membranes for water cleaning: Tailoring of mechanical stability and water flux. *Under revision in Reactive and Functional Polymer*.

Table of Contents

1. Introduction	1
1.1. Nanotechnology based membranes	2
1.1.1 Inorganic nanoparticle based membranes	2
1.1.2. Carbon nanotube based membranes	3
1.1.3. Nanocellulose based membranes	5
1.2. Possibilities and challenges in nanocellulose based membranes	7
1.3. Objective of this work	8
2. Experiment Procedure	9
3. Summary of appended papers	13
4. Conclusion	14
5. Future work	15
6. Acknowledgments	16
7. References	17

1. Introduction

A membrane is nothing but a discrete, thin interface that moderates the permeation of chemical species in contact with it. The main advantages of membrane technology as compared with other unit operations in engineering are related to this unique separation principle, i.e. the transport selectivity of membranes. Separations with membranes do not require additives; they can perform at low temperatures (compared to other thermal separation processes) and at low energy consumption. Also, upscaling and downscaling of membranes processes as well as their integration into separation or reaction process are easy (Ulbricht, 2006).

Membranes can be classified in several ways but pressure-derived membranes are classified according to characteristic pore size or their intended applications (Table 1). Microfiltration (MF) and ultrafiltration (UF) membrane systems have been the most attractive alternatives since they offer quick and selective separation on removing suspended particles, pathogenic agents and dissolved macromolecules, such as proteins and polysaccharides, from water. Nanofiltration (NF) membranes are relatively new and are sometimes called “*loose*” reverse osmosis (RO) membranes. They are generally porous membranes, but as the pores are on the order of nanometers, they revealed performance between that of RO and UF membranes.

Table 1: Membranes characterization by pore types and target species

Pore type (size range/nm)	Membranes types (pore size/nm)	Species ^c	Dimensions ^c /nm
Macropores (> 50)	Microfiltration ^a (50-500)	Yeast and fungi	1000-10000
		Bacteria	300-10000
		Oil emulsions	100-10000
Mesopores (2-50)	Ultrafiltration ^a (2-50)	Colloidal solids	100-1000
		Virus	30-300
		Proteins/Polysaccharides	3-10
Micropores (0.2-2)	Nanofiltration ^a (≤ 2)	Common antibiotics	0.6-1.2
	Reverse osmosis ^b (0.3-0.6)	Organic antibiotics	0.3-0.8
	Forward osmosis ^b (0.3-0.6)	Inorganic ions	0.2-0.4
		Water	0.2

^aUlbricht, (2006) ^bKestine, (1990) ^cMulder, (1996)

1.1. Nanotechnology based membranes

Nanotechnology concepts have led to new nanoscale membranes that exceed state-of-the-art performance and enable new functionality, such as high permeability, catalytic reactivity, and fouling resistance (Theresa et al., 2011). Polymeric membranes fabricated through nanotechnology routes are of great interest because polymers offer great design flexibility and are generally less expensive compared to ceramic membranes.

Since the term “nano” in membrane technology is already assigned to a specific type of membrane (pore size 0.2-2 nm), nanostructured membranes refer to the pore size of the membrane within nano-range (Theresa et al., 2011). “Nano-enabled” (NEM) membranes are the ones engineered with nano-sized particles (inorganic/CNTs/organic). NEM have proven their efficiency in removing particles, bacteria/viruses, (natural) organic matter, hardness, metals (such as arsenic, uranium, lead, chromate), sulphate and a number of organic and inorganic substances (such as pesticides and some pharmaceuticals) sometimes even in one single treatment step (Theresa et al., 2011). The use of nanoparticles in the manufacturing of membranes allows for both a high degree of control over membrane structure and the ability to produce desired stability as well as their functionalities for water purification (Yan et al., 2005; Rahimpour et al., 2010; 2013).

1.1.1. Inorganic nanoparticles based membranes

Nano-alumina

Alumina is one of the inert biomaterials used in membrane fabrication. It is a biodegradable material, well tolerated by the biological environment. Very few studies have been performed to use alumina in nanoscale for water purification. Recently, sodium dodecyl sulfate (SDS) coated nano-alumina composite was developed for the removal of metal cations Pb(II), Cd(II), Cr(III), Co(II), Ni(II) and Mn(II) from water samples by Afkhami et al., (2010). The results displayed that composite has the highest adsorption capacity for Pb(II), Cr(III) and Cd(II) in ions mixture system. Desorption experiments by elution of the adsorbent with a mixture of nitric acid and methanol show that the modified alumina nanoparticles could be

reused without significant losses of its initial properties even after three adsorption–desorption cycles. Thus, modified nano-alumina with SDS is favorable and useful for the removal of these metal ions, and the high adsorption capacity makes it a promising candidate material for Pb(II), Cr(III) and Cd(II) removal.

Nano zeolites

Jawor and Hoek, (2010) have conducted very novel and interesting research related to removal of cadmium ions from water by nanoparticle enhanced ultrafiltration using zeolite nanoparticles within polymeric phase. Complete removal (100%) of cadmium was observed from water. Furthermore, the increase in colloidal zeolite caused relatively little flux decline.

Nano zirconium

Encapsulation of ZrP nanoparticles into macroporous polystyrene with various surface groups, $-\text{CH}_2\text{Cl}$, $-\text{SO}_3^-$, and $-\text{CH}_2\text{N}^+(\text{CH}_3)_3$ were fabricated, respectively for lead removal from water. Effect of functional groups on nano-ZrP dispersion and mechanical strength of resulting nanocomposite were investigated. The presence of charged functional groups are more favorable than neutral group to improve nano-ZrP dispersion. ZrP-N and ZrP-S had higher capacity than ZrP-Cl for lead removal (Zhang et al., 2011).

Silver nanoparticles

Nanocomposite membrane has been fabricated with two-component, consist of a cationic polymer, poly(4-vinyl-N-hexylpyridinium bromide), and embedded silver bromide nanoparticles. Cationic polymer/silver bromide nanoparticle composites showed potent long-lasting antibacterial activity toward both gram-positive and gram-negative bacteria (Sambhv et al., 2006).

1.1.2. Carbon nanotube based membranes

Recently, in a report the fabrication of nanocomposite incorporated with aligned carbon nanotube walls was reported (Srivastava et al., (2004). The study reveals the elimination of multiple components of heavy hydrocarbons from petroleum and the filtration of bacterial contaminants such as *Escherichia coli* or the nanometer-sized

poliovirus (25 nm) from water. These macro filters can be cleaned for repeated filtration through ultrasonication and autoclaving. The exceptional thermal and mechanical stability of nanotubes, and the high surface area, ease and cost-effective fabrication of the nanotube membranes may allow them to compete with ceramic- and polymer-based separation membranes used commercially.

Some common functional nanoparticles have also been reported in the literature have been summarized in table 1. The main aim of incorporation of these nanoparticles was to increase the composite properties as well as their pollutant removal efficiency.

Table 1: Functional membranes for pollutants removal

Membranes	Pollutants	Reference
Carbon nanotubes in polymer	Bacteria and viruses	Srivastava et al. (2004)
Alumina membrane formed from A-alumoxane	Synthetic dyes	DeFriend et al. (2003)
Alumina membranes functionalized with poly(styrene sulfonate) or poly(allylamine hydrochloride)	Divalent cations	Stanton et al. (2003)
Silica and cellulose-based membranes functionalized with amino acid homopolymers	Metal ions	Ritchie et al. (1999, 2001)
Polycarbonate track-etched membranes functionalized with amino acid homopolymers	Metal ions	Hollman and Bhattacharayya (2004)
Pt/Fe laden cellulose acetate film	Trichloroethylene (TCE)	Meyer et al. (2004)
Zero-valent Fe laden cellulose acetate membrane	TCE	Wu et al. (2005)
Alumina or polymeric membranes with gold nanoparticles	4-nitrophenol	Dotzauer et al. (2006)
Polymer-impregnated ceramic TiO ₂ filters	Polycyclic aromatic hydrocarbons (PAHs)	Arkas et al. (2006)
Polymer-impregnated ceramic alumina and silicon-carbon filters	Trihalogen methanes, PAHs,	Allabashi et al. (2007)

	pesticide	
--	-----------	--

1.1.3. Nanocellulose based membranes

The fabrication of nanoenabled composite membranes by incorporation of nanocellulose is a new application area in the field of membrane technology. Dual approach might be used for the filtration of contaminants from water using NEMs: a) physical nanofiltration/ultrafiltration process and b) adsorption by functional entity (nanocellulose). For the first time a research group from Stony Brook University reported nanocellulose as functional entity for the capturing of pollutants present in water (Ma et al., 2011a; 2011b; 2012). Therefore, affinity membranes were developed to permit the purification of contaminants based on physical/chemical properties or biological functions. Rather than operate purely on the sieving mechanism, affinity membrane based on its separation on the selectivity of the membrane to attach contaminants, by immobilizing specific ligands or produce specific functional groups onto the surface of membranes. Affinity membrane reflects technological advances in both fixed-bed liquid separation and membrane filtration, and combines both the outstanding selectivity and the reduced pressure drops associated with filtration membranes.

Hierarchical structures of cellulose

Cellulose is, a polysaccharide consisting of a linear chain of several hundred to over ten thousand β -(1 \rightarrow 4) -linked D-glucose units with the formula $(C_6H_{10}O_5)_n$. Cellulose is widely spread in nature and closely relevant to people's daily life from wood, paper to cotton and flax. For green plants, cellulose is enriched in cell walls with the dry weight content from 40% to 60% (lignin: 10% to 35%, hemicellulose: 20% to 40%). Cellulose as polysaccharide is odorless, nontoxic and hydrophilic (contact angle of 20°-30°) with three hydroxyl groups one each unit (Updegraff. 1969).

Cellulose has hierarchical structure from nano to macro scale (Fig. 1). Cellulose molecular chains were bundled by intra and inter molecular hydrogen bonds formed by hydroxyl groups. Elementary fibrils are in composed of multiple cellulose chains. Cellulose micro fibrils are composed of crystalline section and amorphous section.

One micro fibril contains several elementary fibrils. The micro fibrils are about 10–30 nm wide containing 20,000–30,000 cellulose molecules. The elementary fibrils are upto cell wall.

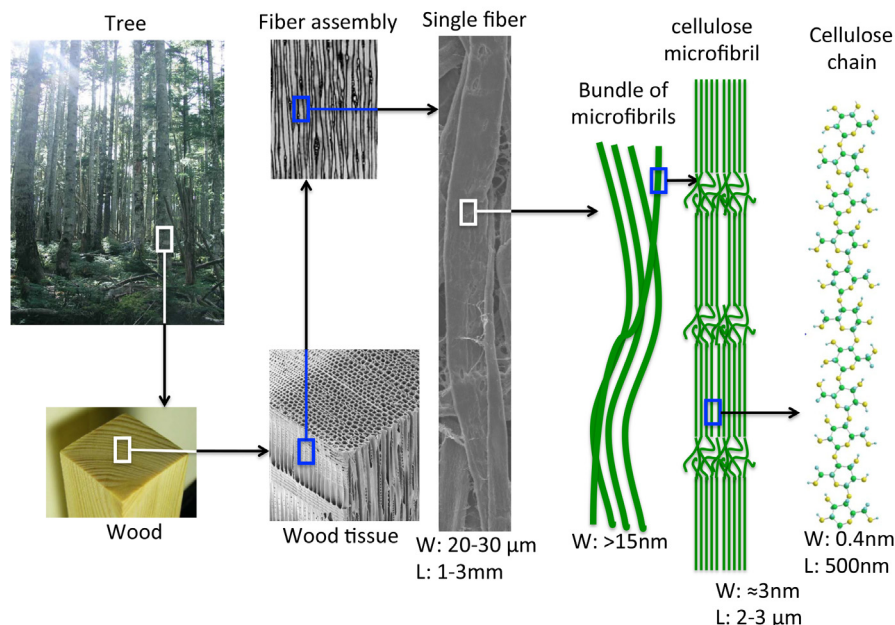


Fig. 1: Schematic of hierarchical structure of wood from macro to nano, Isogai et al. (2011)

Cellulose nanocrystals (CNC) and cellulose nanofibers (CNF)

Cellulose nanocrystals are crystals in the shape of needle (crystal length: 150-300nm, crystal diameter: 1-5 nm). Crystalline cellulose is more chemical resistant than amorphous section. The key procedure to isolate cellulose nanocrystals is to extract cellulose crystalline crystals from amorphous matrix by the method of acid hydrolysis. The theoretical value of Young's modulus along the chain axis for perfect native CNCs is estimated to be 167.5 GPa, which is stronger than steel and similar to kevlar (Tashiro and Kobayashi, 1991), while the experimental elastic modulus of native CNCs were in the range of 105-143 GPa, respectively (Rusli and Eichhorn, 2008; Sturcova et al., 2005, Nishino et al., 1995).

Cellulose nanofibers could be treated as cellulose fibrils obtained by fibrillation. The indispensable procedure of preparing CNF is mechanical treatment such as sonification, homogenization or ultrafine grinding. High-energy input is required to

get cellulose fibrillated. In some cases, pretreatment (enzymatic pretreatment, chemical pretreatment or mechanical pretreatment) is carried on to prepare CNF in order to reduce energy input or enhance CNF quality. However, the preparation method of CNF largely depends on raw materials and the expectation of CNF quality (Jonoobi et al., 2012). Nanocrystals are much shorter than nanofibers (Oksman et al., 2011). CNF contain both crystalline and amorphous sections with the diameter of 10-70 nm and the length of $\geq 1\mu\text{m}$. Despite the presence of amorphous portion along their length, the tensile strength of these nanofibers is supposed to be around 2 GPa, based on the strength of pulp single fiber (Page and El-Hosseiny, 1983).

1.2. Possibilities and challenges in nanocellulose based membranes

Nanocellulose has gained increasing attention due to the high strength, stiffness, biodegradability and renewability, and drastic increase in physical and functional properties in polymeric composites. Because of the equatorial positions of the hydroxyls on the cellulose chain, they protrude laterally along the extended molecule and are readily available for hydrogen bonding. These hydrogen bonds cause the chains to group together in a highly ordered structure, which make them mechanically stable. Good mechanical strength and rigidity can offer resistance to high-pressure environmental for the membranes in real water purification application.

Nanocelluloses are highly crystalline lattice structure, which provide the possibility to work within different pH ranges. Oksman et al., (2011) reported the crystallinity of nanocelluloses to be in the range of 70-80% depending on the process of isolation. Further more, the high crystallinity value makes them resistant to acid wash (regeneration of composite membranes and recovery of valuable pollutants).

Stability in water environment as well as hydrophilicity of nanocellulose is also an advantage while using in water treatment. The hydrophilicity is expected to reduce bio-fouling and organic fouling. Yet, owing to their hydrophilic nature, their utilization in membrane application involving hydrophobic media is restricted, which limit their exploitation in non-aqueous medium.

High surface area of nanocellulose provides large number of active sites for the interaction and immobilization of pollutants. Recently, Sehaqui et al., (2011) reported a surface area of $482\text{ m}^2\text{ g}^{-1}$ for nanopaper prepared using supercritical CO_2 drying. However, it will be challenging to maintain this high surface area during membrane

processing.

With the presence of large number of chemical functionality within their structure, these building blocks provide a unique platform for significant surface modification through various chemistries (Habibi, 2014). The introduced functional groups can be tailored for the binding of specific/desirable pollutants from water. Volesky (2007) summarized that functional groups such as carbonyl (ketone), carboxyl, sulfhydryl (thiol), sulfonate, thioether, amine, and secondary amine, phosphate, phosphodiester and imidazole etc. on various bio-residues are responsible for pollutant removal. Liu et al have shown that the presence of COO^- , SO_3^- , PO_3^{2-} on the surface of nanocellulose makes them selective towards the positively charged species (Liu, 2014).

In spite of various advantages, the use of nanocellulose in polymeric phase also creates some hurdles: a) homogenous dispersion, b) fouling (biological and chemical), c) regeneration, d) recovery etc.,

1.3. Objective of this work

There are various conventional techniques for the wastewater treatment but all of them have some demerits such as high cost operation, incomplete pollutants removal, sludge disposal etc. For example, the removal of metal ions by chemical precipitation or electrochemical treatment is usually inefficient, when ions concentration is among 1 to 100/ mg because the unit of copper in drinking water recommended by WHO is 2 mg/L, which is not possible to achieve by precipitation (Liu et al., 2014). And during the process, large quantity of sludge is procured and required to be treat again with great difficulties.

Numerous nanocomposites have been applied in abatement of contaminants from various environmental media like groundwater, drinking water and industrial effluents but none of them are fully biobased. The objective of this work is to explore the scale up of nanocrystals production and processing of fully biobased nanocomposite membranes using nanocrystals as functional entities. The composite membranes were characterized to understand the behavior of nanocrystals within matrix. Finally, the adsorption behavior of dyes and heavy metals ions on the membranes was also studied. To improve the adsorption behavior, surface modified nanocrystals were also used in this study.

2. Experimental procedure

Materials and methods

Two biomass materials namely cellulose sludge and wood chips are used for the preparations of nanocrystals. Raw materials used are bioresources with low or even negative cost.

Cellulose sludge supplied by Domsjö Fabrikerna AB, Örnsköldsvik, Sweden was used as the raw material for the preparation of CNC_{SL}. The cellulose sludge was reported to be high in cellulose (95%) with some hemicellulose and trace amounts of lignin (Jonoobi et al., 2012). The cellulose sludge was used without any pre-treatment for isolation of nanocellulose.

Unbarked wood chips of Norway spruce (*Picea abies*) with a dry matter content of 50-55% were used as the raw material for the processing of cellulose nanocrystals (CNC_{BE}). The cellulose was obtained by dilute acid hydrolysis at the pilot-scale facility at SEKAB, Örnsköldsvik, Sweden, and subsequent refining with solvent extraction and delignification (performed by More Research Örnsköldsvik, Sweden). The cellulose was provided as suspensions of 17% concentration and used for isolation into cellulose nanocrystals by homogenization.

The CNC_{SL} were enzymatically modified in a reaction mixture and renamed as PCNC_{SL}. Reaction was carried out accordingly to Bozic et al. (2014).

The methods used to isolate the nanopolysaccharides used in this study are displayed in Fig. 2.

Surface functionality based on process route

The isolation pathways of nanocelluloses are responsible for the introduction of functional groups. The isolation of CNC_{SL} was performed by sulphuric acid hydrolysis (Bondeson et al., 2006) and sulfonate groups (SO₃⁻) were achieved. Thus, the isolation of CNC_{SL} via sulphuric acid hydrolysis introduces a minor amount of sulfonate groups which yield negative charge that promote a perfectly uniform dispersion of CNC_{SL} in water via electrostatic repulsion.

CNC_{BE} was prepared by homogenization of cellulose prepared using bioethanol process as reported by Oksman et al. (2011). The main functional group that appear after isolation process was carboxylate ($-C=OO^-$).

The introduction of phosphate (PO_3^{2-}) group on the surface of CNC_{SL} was performed using hexokinase-mediated reaction and modified nanocellulose were denoted as PCNC_{SL} (Bozic et al. 2014).

The roadmap to develop the nanocrystals and the functional groups available on the surface are summarized in Fig. 3.

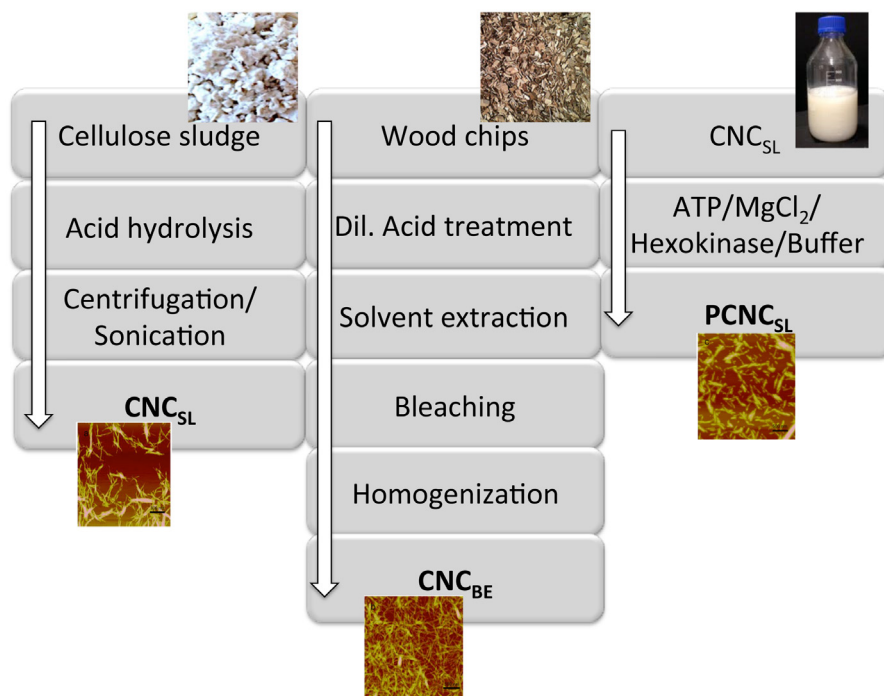


Fig 2. Procedure for isolation and modification of nanocrystals

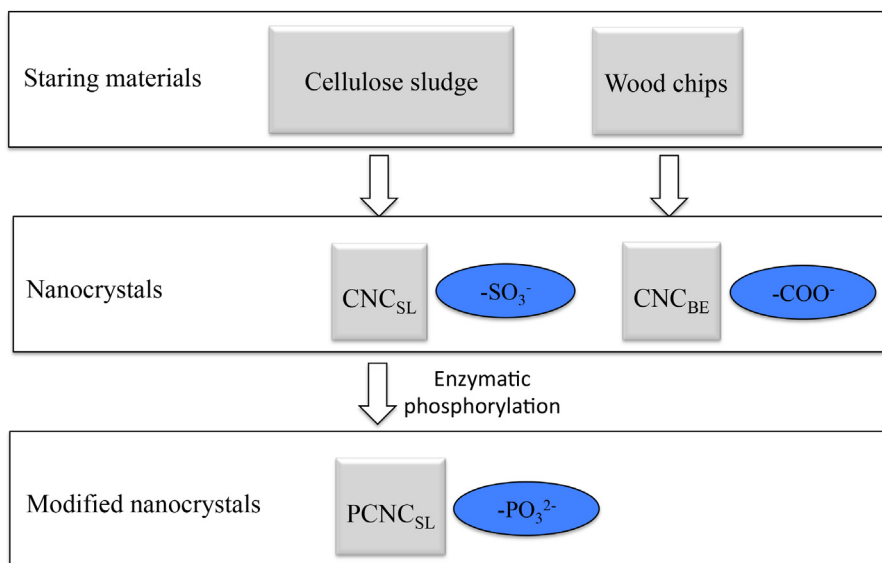


Fig. 3 Road map showing the raw materials, isolated nanocrystals and the derivatives (p-: phosphorylated)

Characterizations of composite membranes

Atomic force microscope (AFM) and scanning electron microscopy (SEM) were utilized to observe nanocrystals and composite membranes morphologies, respectively. X-ray diffraction (XRD) reveals the crystallinity of the nanocrystals. Zeta sizer has been used to understand the surface charge content and Z potential of these nanocrystals and X-ray photoelectron Spectroscopy (XPS) for surface groups. Mechanical properties of composite membranes were measured using tensile machine. The specific surface area and average pore size of fabricated nanocomposite membranes were determined by Brunauer-Emmett-Teller (BET) and bubble point measurement instrument respectively. Attachment of functional groups and formation of new bonds with nanocrystals and matrix were analyzed by Fourier Transform Infrared Spectroscopy (FTIR).

Flux measurement

A dead-end stirred cell filtration system connected with an N₂ gas cylinder was used to evaluate the flux performance of the composite membranes. Experiments were carried out using a filtration test cell, Dead End Cell (Sterlitech HP4750 Stirred cell,

USA) with a capacity of 300 ml. This study was considered as lab scale and the membrane area used for the measurement was 0.001886 m^2 .

The cross flow filtration device consists of a feed tank with a total working volume of 10L and a filtration module was further used to measure the flux of composite membranes. Thin-layered composite membranes were stored in a 10L feed tank and then placed in a module connected to a recirculation loop, where a diaphragm pump sustained the recirculation flow rate. A backpressure valve was located in the recirculation loop to adjust the trans-membrane pressure. This measurement was at scale and performed in collaboration with AlfaLaval AB, Sweden, The membrane area used was 0.0336 m^2 .

Evaluation of adsorption behavior

In this study, the primary goal was to evaluate the properties and behavior of fabricated composite membranes that are relevant to or affecting adsorption behavior towards metal ions.

Adsorption experiments are conducted to study the contaminants (dyes and metal ions) removal efficiency by the nanocomposite membranes. Percentage removal of dyes was calculated by measuring absorbance using UV-visible spectroscopy at respective wavelength. Adsorption capacity and metal removal percentage was calculated by the solution concentration differences of the metal ions before and after adsorption using inductively coupled plasma-optical emission spectrometer (ICP-OES). The adsorbed metal ions on the surface of composite membranes were further demonstrated by X-ray electron microscopy (EDS).

3. Summary of appended papers

Paper A: Process scale up and characterization of wood cellulose nanocrystals hydrolysed using bioethanol pilot plant

This study shows the isolation and scale up of a cellulose nanocrystals, CNC_{BE}. The scaled up production of CNC_{BE} was made possible by integrating the acid hydrolysis in pilot scale bioethanol plant with lab scale homogenization. The diameter of isolated nanocrystals was in the range of 5-15 nm, a cellulose 1 crystalline structure and transparent at low concentration. Isolated nanocrystals have negative surface charges as measured by zeta sizer and attributed to the presence of carboxylic group as evidenced by XPS study. The fabricated films of CNC_{BE} nanocrystals showed enhanced mechanical, optical and cytocompatible properties compared to sulphuric acid hydrolyzed nanocrystals, CNC_{SL}. The process route developed for the isolation of CNC_{BE} is novel and enabled a yield of 600g/day for nanocrystals.

Paper B: Nanoporous membranes with cellulose nanocrystals as functional entity in chitosan: Removal of dyes from water

The use of nanocrystals as functional entity within a matrix is a novel approach for the wastewater treatment. In this study, chemically isolated nanocrystals (CNC_{SL}) was used to make membrane like 3D structure within chitosan network and was further stabilized by cross-linking. The developed membranes were in ultrafiltration range and had pore sizes of 7-9 nm. The higher efficiency for the removal of dyes was observed, being the highest for Victoria Blue (98%), followed by Methyl Violet (90%) and Rhodamine 6G (78%). Two mechanisms were proposed for dyes adsorption onto the membrane, hydrogen bonding and electro-static interaction. The dyes adsorption behavior of composite membranes was found to be pH dependent and the best adsorption performance was observed near neutral pH. Furthermore, the membranes showed low flux (64 L m⁻²h⁻¹MPa), which supports the usefulness of composite membranes as adsorbents. The high efficiency of the membranes, in terms of adsorption was attributed the freeze-drying process used, which resulted in well individualized CNCs which act as functional entities that are loosely bound together by chitosan polymer chains locked in a 3D network via cross-linking. It may however be noted that freeze-drying adversely affected the mechanical performance of the

membranes and will be addressed in the future studies.

Paper C: High flux affinity membranes based on cellulose nanocomposite for removal of heavy metal ions from industrial effluent

Very fast and scalable process, vacuum filtration has been used for the fabrication of fully biobased composite membranes and were successfully used for $\approx 100\%$ removal of heavy metal ions from mirror industry effluents. Layered composite membranes were fabricated using cellulose sludge as support layer and three nanocrystals (CNC_{SL} , CNC_{BE} , PCNC_{SL}) in gelatin matrix as functional layer. The use of sludge as support layer not only cut down the cost of composite membranes but also provided the mechanical stability. SEM studies confirmed the individualized nanocrystals in the functional layer and the bi-layered morphology of nanocomposite. The membranes had a tensile strength of 16 MPa in dry conditions and a wet strength of 0.2 MPa, which is sufficient for using these membranes in spiral wound modules. Mirror making industry effluent laden with metal ions (Ag^+ and $\text{Cu}^{2+}/\text{Fe}^{3+}$) was incubated with composite membrane to evaluate the metal ion removal capability. Sorption capacity of PCNC_{SL} was highest being 100% removal for all metal ions; followed by CNC_{BE} than CNC_{SL} . The removal of metal ions was expected to be driven by the electrostatic attraction between negatively charged nanocellulose and the positively charged metal ions. Bubble point measurements confirmed that the membrane pore structure was in microfiltration range (5.0 -6.1 μm), which provided very high water permeability (900-4000 $\text{Lh}^{-1}\text{m}^{-2}$) at pressures of <1.5 bars.

4. Conclusion

The current studies have proved that a new scaled up process of nanocrystals isolation integrated with bioethanol production route is possible. The isolated nanocrystals have negative zeta potential due to the presence of carboxylic group on the surface, confirmed by XPS. The fabricated film shows better properties as compared to the CNC_{SL} film. CNC_{BE} is considered to have significant advantage in membrane fabrication due to its availability in larger scale, higher surface negative charge, better film properties etc

The use of nanocrystals as functional entities for the removal of contaminants from wastewater is new approach; to prove that, nanostructured composite membranes

have been fabricated by freeze-drying method and vacuum filtration method. The developed membranes showed high removal efficiency for dyes from model water as well as metal ions from industrial water. Adsorption efficiency of nanocrystals can be dramatically enhanced by enzymatic phosphorylation. The phosphorylated nanocrystals based membranes successfully reduced the metal ions concentration (Ag^+ , Cu^{2+} , Fe^{3+}) to the acceptable limits for fresh water based on WHO regulations. In all cases the adsorption was found to be pH dependent which correlates with adsorption/ desorption performance and potential for recovery of valuable contaminants.

It was found that freeze-drying resulted in the nanocomposite membranes with nanoscaled porosity but low stability due to the absence of hydrogen bonding. Vacuum filtration method in the other hand resulted in membranes with higher mechanical properties and micron scaled porosity. Further more, thin layer of dense functional layer on a highly porous substrate provides high flux and mechanical stability even in wet conditions.

The low cost of the used bioresources, scaling up potential of nanocrystals, the functional performance of their membranes are expected to result in commercially viable and fully biobased membranes for water purification.

5. Future work

Freundlich and Langmuir adsorption isotherm for metal ions and dyes will be good start to understand the saturation limit and capacity of composite membranes. Furthermore, the effect of temperature, incubation time and dose of pollutants could be easily studies on adsorption reaction in static mode.

Another approach will be the understanding of correlation between the applied pressure with permeation flux and porosity of used composite membranes in dynamic mode. Furthermore, pre-prediction of relationship between the thicknesses of composite membranes with respect to flux with constant applied pressure could be studied in future.

In the long run, the goal is to produce commercially competitive composite membranes to immobilize heavy metal ions for water purification. Therefore studies will focus on scale up the processing of nanocomposite membranes up to prototype level using flat sheet membranes and spiral modules.

6. Acknowledgments

I acknowledge the financial support of the European Commission, under the NanoSelect Project, EU FP7-NMP4-SL-2012- 280519.

I would like to thank SEKAB E-Technology, Domsjö Fabrikerna AB, More Research, SP Processum, Örnsköldsvik, Sweden for all supplied raw materials. I would like to thank Desiree Nordmark, LTU, Sweden for ICP-OES studies.

Iftekhar Uddine Bhuiyan has been highly acknowledged for SEM analysis

My sincere appreciation to all my colleagues for offering me help inside and outside the lab.

I would like to thank my family for their support.

7. References

- Afkhami, A., Saber-Tehrani, M. Bagheri, H. Simultaneous removal of heavy-metal ions in wastewater samples using nano-alumina modified with 2,4-dinitrophenylhydrazine. *J. Hazardous Mat.* (2010); 181: 836-844.
- Allabashi, R., Arkas, M., Hörmann, G., Tsiourvas, D. Removal of some organic pollutants in water employing ceramic membranes impregnated with cross-linked silylated dendritic and cyclodextrin polymers. *Water Res.* (2007); 41: 476–486.
- Arkas, M., Allabashi, R., Tsiourvas, D., Mattausch, E. M., Perfler, R. Organic/inorganic hybrid filters based on dendritic and cyclodextrin “nanosponges” for the removal of organic pollutants from water. *Environ. Sci. Technol.* (2006); 40: 2771–2777.
- Baley, C. Analysis of the flax fibres tensile behaviour and analysis of the tensile stiffness increase, *Composites Part A* (2002); 33: 939–948.
- Bondeson, D., Mathew, A., Oksman, K. Optimization of isolation of nanocrystals from microcrystalline cellulose by acid hydrolysis. *Cellulose* (2006); 13: 171–180.
- Bos, H. L., van-den-Oever, M. J. A., Peters, O. C. J. J. Tensile and compressive properties of flax fibres for natural fibre reinforced composites. *J. Mat. Sci.* (2002); 37: 1683–1692.
- Bozic, M., Peng, L., Aji, P. M., Kokol, V. Enzymatic phosphorylation of cellulose nanofibers to new highly-ions adsorbing, flame-retardant and hydroxyapatite-growth induced natural nanoparticles. *Cellulose* (2014); 21:2713-2726.
- DeFriend K. A., Wiesner, M. R., Barron A. R. Alumina and aluminate ultrafiltration membranes derived from alumina nanoparticles. *J. Memb. Sci.* (2003); 224: 11–28.

Dotzauer, D. M., Dai, J., Sun, L., Bruening, M. L. Catalytic membranes prepared using layer-by-layer adsorption of polyelectrolyte/metal nanoparticle films in porous supports. *Nano Let.* (2006); 6: 2268–2272.

Habibi, Y. Key advances in the chemical modification of nanocelluloses. *Chem. Soc. Rev.* (2014); 21: 345-387.

Hollman A. M., Bhattacharyya D. Pore assembled multilayers of charged polypeptides in microporous membranes for ion separation. *Langmuir* (2004); 20: 5418–5424.

Isogai, A., Satio, T., Fukuzumi, H. TEMPO oxidized cellulose nanocrystals. *Nanoscale* 2011; 3: 71-85.

Jawor, A., Hoek, E. M. V. Removing cadmium ions from water via nanoparticle-enhanced ultrafiltration, *Environ. Sci. Technol.* (2010); 44: 2570–2576.

Jonoobi, M., Mathew, A. P., Oksman, K. Producing low cost cellulose nanofiber from sludge as new source of raw materials. *Ind. Crops Prod.* (2012); 40: 232–238.

Kesting, R. E. The 4 tires of structure in integrally skinned phase inversion membranes and their relevance to various separation regimes, *J, Appl. Polym, Sci*, (1990), 41: 2739-2752.

Lamy, B., Baley, C. Stiffness prediction of flax fibers-epoxy composite materials. *J. Mat. Sci. Let.* (2000); 19: 979–980.

Liu P. Nanopolysaccharides for adsorption of heavy metals ions from water. (2014), Licentiate thesis, LTU, Sweden.

Ma, H., Burger, C., Hsiao, B. S., Chu, B. Highly permeable polymer membranes containing channels for water purification. *ACS Macro Let.* (2012); 1: 723-726.

- Ma, H., Burger, C., Hsiao, B. S., Chu, B. Ultra-fine cellulose nanofibers: New nano-scale materials for water purification. *J. Mat. Chem.* (2011a); 21: 7507–7510.
- Ma, H., Burger, C., Hsiao, B. S., Chu, B. Ultrafine polysaccharide nanofibrous membrane for water purification, *Biomacromolecules* (2011b); 12: 970–976.
- Meyer, D. E., Wood, K., Bacha, L. G., Bhattacharyya, D. Degradation of chlorinated organics by membrane-immobilized nanosized metals. *Environ. Prog.* (2004); 23: 232–242.
- Mulder, M. *Basic Principle of Membranes Technology*, Kluwer Academic Publishers, London, (1996).
- Nishino, T., Takano, K., Nakamae, K. Elastic modulus of the crystalline regions of cellulose polymorphs. *J. Polym. Sci. Part B: Polym. Phys.* (1995); 33: 1647-1651.
- Oksman, K., Etang, J. A., Mathew, A. P., Jonoobi, M. Cellulose nanowhiskers separated from a bio-residue from wood bioethanol production. *Bio. Bioen.* (2011); 35: 146e152.
- Page, D. H., El-Hosseiny, G. The mechanical properties of single wood pulp fibers. Part VI. Fibril angle and shape of stress-strain curve. *J. Pulp. Pap. Sci.* (1983); 84: 99-100.
- Rahimpour, A., Jahanshahi, M., Rajaeian, B., Rahimnejad, M. TiO₂ entrapped nano-composite PVDF/SPES membranes: Preparation, characterization, antifouling and antibacterial properties. *Desalination* (2013); 16, 225-335.
- Rahimpour, A., Madaeni, S. S., Mansourpanah, Y. Nano-porous polyethersulfone (PES) membranes modified by acrylic acid (AA) and 2-hydroxyethylmethacrylate (HEMA) as additives in the gelation media. *J. Mem. Sci.* (2010); 364: 380-388.
- Ritchie, S. M. C., Bachas L. G., Olin, T., Sikdar, S. K., Bhattacharyya, D. Surface modification of silica- and cellulose-based microfiltration membranes with functional polyamino acids for heavy metal sorption. *Langmuir* (1999); 15: 6346–6357.

Ritchie, S. M. C., Kissick, K. E., Bachas, L. G., Sikdar, S. K., Parikh, C., Bhattacharyya, D. Polycysteine and other polyamino acid functionalized microfiltration membranes for heavy metal capture. *Environ. Sci. Technol.* (2001); 35: 3252–3258.

Rusli, R., Eichhorn, S. J. Determination of stiffness of cellulose nanowhiskers and the fiber-matrix interface in a nanocomposite using raman spectroscopy. *Appl. Phys. Lett.* (2008); 93: 3-14.

Sambhy, V., MacBride, M., Blake, R., Sen, A. Silver bromide nanoparticle/polymer composites: Dual action tunable antimicrobial materials. *J. Am. Chem. Soc.* (2006), 128, 9798-9808.

Sehagui, H., Zhou, Q., Ikkala, O., Berglund, L. A. Strong and tough cellulose nanopaper with high specific surface area and porosity. *Biomacromolecules* (2011); 12: 3638–3644.

Sharma, Y., Srivastava, C. V., Singh, V. K., Kaul, S. N., Weng, C. H. Nano-adsorbents for the removal of metallic pollutants from water and wastewater, *Environ. Technol.* (2009); 30: 583–609.

Srivastava, A., Srivastava, O., Talanatra, S., Vaital, R., Aiayan, P. M. Carbon nanotube filters. *Nature Mater* (2004); 3: 610–614.

Stanton, B. W., Harris, J. J., Miller, M. D., Bruening, M. L. Ultrathin, multilayered polyelectrolyte films as nanofiltration membranes. *Langmuir* (2003); 19: 7038–7042.

Sturcova, A., Davies, G. R., Eichhorn, S. J. (2005). Elastic modulus and stress-transfer properties of tunicate cellulose whiskers. *Biomacromolecules* (2005); 87: 2038-2045.

Tashiro, K., Kobayishi, M. Theoretical evaluation of three- dimensional elastic constants of native and regenerated celluloses: role of hydrogen bonds. *Polymer* (1991); 32: 1516–1521.

Theresa, M., Pendergast, M., Eric, M. V. Hoek. A review of water treatment membranes technologies. Eng. Environ. Sci. (2011); 4: 1946-1971.

Ulbricht, A. Advanced functional polymeric membranes, Polymer (2006); 47: 2217-2262.

Updegraff, D. M. Semimicro determination of cellulose in biological materials. Analy. Biochem. (1969); 32: 420-424.

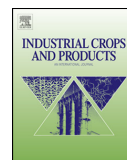
Volesky, B. Biosorption and me. Water Res. (2007); 41: 4017-4029.

Wu, L., Shamsuzzoha, M., Ritchie S. M. C. Preparation of cellulose acetate supported zero-valent iron nanoparticles for the dechlorination of trichloroethylene in water. J. Nanopart. Res. (2005); 7: 469-476.

Yan, L., Li, Y. S., Xiang, C. B. Preparation of poly(vinylidene fluoride) (PVDF) ultrafiltration membrane modified by nano-sized alumina (Al_2O_3) and its antifouling research, Polymer (2005); 46: 7701-7706.

Zhang, Q., Pan, B., Zhang, S., Wang, J., Zhang, W., Lu, L. New insights into nanocomposite adsorbents for water treatment: A case study of polystyrene-support zirconium phosphate nanoparticles for lead removal. Nanopart Res. (2011); 13: 5355-5364.

Paper A



Process scale up and characterization of wood cellulose nanocrystals hydrolysed using bioethanol pilot plant

Aji P. Mathew*, Kristiina Oksman, Zoheb Karim, Peng Liu, Saad Ahmed Khan, Narges Naseri

Composite Centre Sweden, Division of Materials Science, Luleå University of Technology, 97187 Luleå, Sweden

ARTICLE INFO

Article history:

Received 27 November 2013
Received in revised form 8 March 2014
Accepted 17 April 2014
Available online 9 May 2014

Keywords:

Cellulose nanocrystals
Scale up
mechanical properties
X-ray photoelectron spectroscopy
wood

ABSTRACT

The paper discusses the isolation of cellulose nanocrystals (CNC_{BE}) from wood resources by integrating the processing with pilot-scale bioethanol processing unit. The nanocrystals were isolated from cellulose obtained by acid pretreatment of wood chips in a bioethanol pilot-scale facility, followed by a series of chemical processes and subsequent homogenization using a lab-scale homogenizer. The isolated nanocrystals had diameters of 5–15 nm, cellulose I crystalline structure and formed a thick semi-transparent gel at low concentration (2 wt%). XPS data showed that these nanocrystals had predominantly O=C–O surface groups which also contributed to its high negative zeta potential. Casted CNC_{BE} films showed excellent mechanical performance (200 MPa of strength, 16 GPa of modulus) and transparency and were also found to be cytocompatible. The developed process route resulted in high-quality nanocellulose crystals with a yield of 600 g/day.

© 2014 Elsevier B.V. All rights reserved.

1. Introduction

Nanocellulose was isolated from natural resources following a top-down approach, taking advantage of its natural hierarchical structure. Isolation and use of biobased nanomaterials has been an area of great interest in materials science research during the last few decades.

Since the first reports on cellulose nanocrystal isolation from wood pulp by Rånby in the 1950s, several natural resources like wheat straw, crab shell, tunicates, plant fibres, etc., have been used by researchers to prepare nanocrystals via chemical processes (Rånby, 1952; Dufresne, 2008; Marchessault, 1959; Samir, 2005; Eichhorn et al., 2010; Mathew et al., 2009; Siro and Plackett, 2010). The chemical process involves the removal of the amorphous region from cellulose using either sulphuric acid or hydrochloric acid and subsequent neutralization and individualizing of nanocrystals using ultrasonication. The earlier reports also point to the fact that the ease of isolation, yield of the isolation process as well as the dimensions of the isolated nanocrystals depend on the raw material source. Wood can provide good yield compared to lower plants and agricultural sources, as wood has about 40% cellulose content (Hon, 1996; Han and Rowell, 1996). Furthermore, refined cellulose raw material from industry which can be directly isolated

to cellulose nanocrystals without any specific purification step can provide higher yield. In this context, raw material sources of interest were wood pulp, MCC, etc, which are commercial grades of cellulose with high purity. Many studies report the use of these commercial cellulose sources as starting material for processing of cellulose nanocrystals and nanofibres with high yield efficiency (Edgar and Gray, 2003; Bondeson et al., 2006). Our earlier study on MCC (Bondeson et al., 2006) resulted in processing of CNC at a rate of 50 g/week (with 30% yield w.r.t. initial weight) and provided an improved yield compared to processing of CNC from bioresources like tunicates, wheat straw, etc.

In the recent years, there have been increased efforts to scale up the processing and enhance the efficiency and economy of nanocellulose isolation. CNC isolation in large scale has been reported in recent years because economical and efficient processing of CNC is essential for utilizing CNC as reinforcement or functional additive in commercial products. Most of these attempts to scale up processing have been made in Canada and the USA. For example, FP Innovations Canada reported a production rate of 3 kg/day, CelluForce Canada 1000 kg/day and FPL, US Forest Services 50 kg/week, following a sulphuric acid hydrolysis process (FutureMarkets, 2012; Chauve and Bras, 2014).

Bioresidues and industrial side-streams are of interest in this context and Oksman and co-workers have reported the use of different by-products or residues from forest industries as potential sources for nanocellulose production economically or even at negative cost (Oksman et al., 2011; Jonoobi et al., 2012; Herrera et al.,

* Corresponding author. Tel.: +46 920493336.

E-mail address: aji.mathew@ltu.se (A.P. Mathew).

2012a,b). Cellulose nanocrystals were also isolated from bioethanol residue by mechanical treatments like homogenization or sonication and showed similar properties as nanocrystals isolated from other sources by acid hydrolysis (Oksman et al., 2011; Herrera et al., 2012b). These raw materials were considered as potential sources for isolation of CNCs in large scale.

The current study aims to prepare nanocellulose in bench scale by integrating the lab-scale process with pilot-scale processes existing in wood-based industries. The cellulose obtained from acid hydrolysis using a pilot-scale bioethanol unit was isolated into nanocellulose by mechanical processes in the laboratory. The isolation efficiency, scaling-up potential and quality of final product were evaluated. The properties of the isolated materials and their potential applications in reinforced composites or functional materials are evaluated using mechanical testing, surface characteristics, transparency and cytocompatibility studies. It is expected that scaled-up production of nanocellulose from residues economically and efficiently, with good mechanical and functional properties will facilitate the commercial scale processing of biobased nanostructured products.

2. Experimental

2.1. Materials

Unbarked wood chips of Norway spruce (*Picea abies*) with a dry matter content of 50–55% were used as the raw material for the processing of cellulose nanocrystals (CNC) following the bioethanol processing route at the pilot-scale facility at SEKAB, Örnsköldsvik, Sweden.

The other chemicals used, NaOH, NaClO₂, toluene, sulphuric acid (96%), etc., are of reagent grade and were purchased from VWR, Sweden.

2.2. Methods

2.2.1. Isolation of cellulose nanocrystals

The isolation process is summarised in Fig. 1. Unbarked wood chips of Norway spruce (*Picea abies*) with a dry matter content of 50–55% were treated in a continuous mode with sulphur dioxide in a 30 l reactor at a temperature of 200 °C, at a pressure of 20 bars, and with a residence time of 7 min. 3% (w/w) of SO₂ was used as catalyst. The pH after pre-treatment was about 2 and the total solids content was 28–30%. The slurry was then diluted with water to facilitate pumping and the water insoluble solids content of the diluted slurry was about 17%. The solid material of the slurry was then separated from the liquid using a membrane filter press. The solid material was stored in plastic bags at 4 °C for subsequent use.

The product obtained had cellulose and high amount of lignin and some extractives, which was refined to pure cellulose following TAPPI test method T204 for extraction of cellulose (TAPPI T204).

The first step to purify the solid matter obtained from the bioethanol plant, was the Soxhlet extraction for 6 h at 150 °C using toluene/acetone mixture (2:1 ratio), where by extractives were removed. This material was then bleached using a mixture of 700 ml deionised water, 1.5 ml acetic acid, 6.7 g sodium chlorite, at 70 °C for 12 h. Four further additions of acetic acid and sodium chlorite were made every 2 h and kept for another 12 h, where by a pure white material was obtained. After 24 h of bleaching the materials were washed with excess of deionized water and concentrated to 17 wt% solid content by centrifugation. The FTIR data of the product obtained after this process showed typical cellulose structure with peaks at 3350 cm⁻¹, 2929 cm⁻¹, 1312 cm⁻¹ and 1057 cm⁻¹ of C–H stretching, C–H bending and C–O stretching bonds of cellulose (spectrum not shown), being also verified in our earlier report

where cellulose was isolated from bioethanol residue following this process route (Oksman et al., 2011).

The purified cellulose was made into 2 wt% suspensions, mixed well with shear mixture and passed through the APV 2000 high-pressure homogenizer (Denmark) at a pressure of 500 bars. The suspension with a batch size of 2 l was passed through the homogenizer 10 times to obtain a thick gel of nanocrystalline cellulose, and the processing time was 40 min per batch. This product obtained is denoted as CNC_{BE}.

CNC was also prepared from wood pulp by sulphuric acid hydrolysis in lab-scale, following the procedure reported by Bondeson et al. (2006) and was used as reference. The sulphuric acid hydrolyzed nanocrystals prepared in lab-scale is denoted as CNC_{H₂SO₄}.

2.2.2. Nanofilms and nanopaper preparation

Thin films and nanopaper mats of CNC_{BE} were prepared using (a) casting and (b) filtration and pressing processes, respectively.

Casted films were prepared by drying 40 ml of 1% suspensions of CNC under ambient conditions for approximately 48 h in petri dishes. The resultant films had thicknesses in the range of 100–200 microns.

Nanopaper mats were prepared by vacuum filtration of 120 ml of 0.5% suspension using Whatman filter paper (Pore size number 3 and 125 mm diameter) at –1.0 bar. The CNC filter cakes were dried in ambient temperature under 30 N load for 3 days to keep the nanopaper wrinkle free. The resultant nanopaper mats had thicknesses in the range of 600–700 microns.

CNC_{H₂SO₄} films were prepared only via the casting method, due to experimental difficulties with the filtration and pressing process with this material.

2.3. Characterization

Optical microscopy images of the nanoparticle suspensions were collected using a Leica Optical Microscope using suspension of 0.1 wt%. An atomic force microscope, Nanoscope V, Veeco Instruments (Santa Barbara, CA, USA), was used to examine the morphologies of the CNC_{BE}. A drop of diluted suspensions of each sample was deposited onto freshly cleaved mica and left to dry at room temperature. All the samples were imaged in tapping mode. Height, amplitude and phase images were recorded. The instrument was operated at a resonance frequency of 350 kHz and a spring constant of 10–200 nm⁻¹. The diameter measurements were conducted by Nanoscope V software.

Viscosity of the CNC gels were measured using a Vibro Viscometer (SV 10/SV 100, A&D Company, Ltd, Japan) at 22 °C. Measurements were recorded until the viscosity values were stable and the values were reported after 30 min.

The thermal stability of the nanomaterials was studied by thermogravimetric analysis Q500 (TGA), TA Instruments (New Jersey, USA), at a temperature range of 30–500 °C in an air atmosphere. The temperature was increased at a rate of 10 °C/min and the sample weight was 5–10 mg. All thermal stability curves show the calculated average values and each sample was tested in triplicate.

The zeta potentials of the materials at different pH were measured using a Zetasizer nano ZS, Malvern, at 25 °C. The concentrations of all measured samples remained the same at 0.05 wt%.

X-ray photoelectron spectroscopy (XPS) was used to understand the surface groups on the produced nanocrystals. All XPS spectra were collected with Axis Ultra DLD electron spectrometer (Kratos Analytical Ltd, UK) using monochromatized Al K α (1486.6 eV) radiation. Survey spectra were collected from 1100 to 0 eV at pass energy of 160 eV. High resolution C 1s, O 1s, F 1s and Si 2p spectra were collected at pass energy of 20 eV with a scan step of 0.1 eV. In order to minimize possible X-ray induced degradation

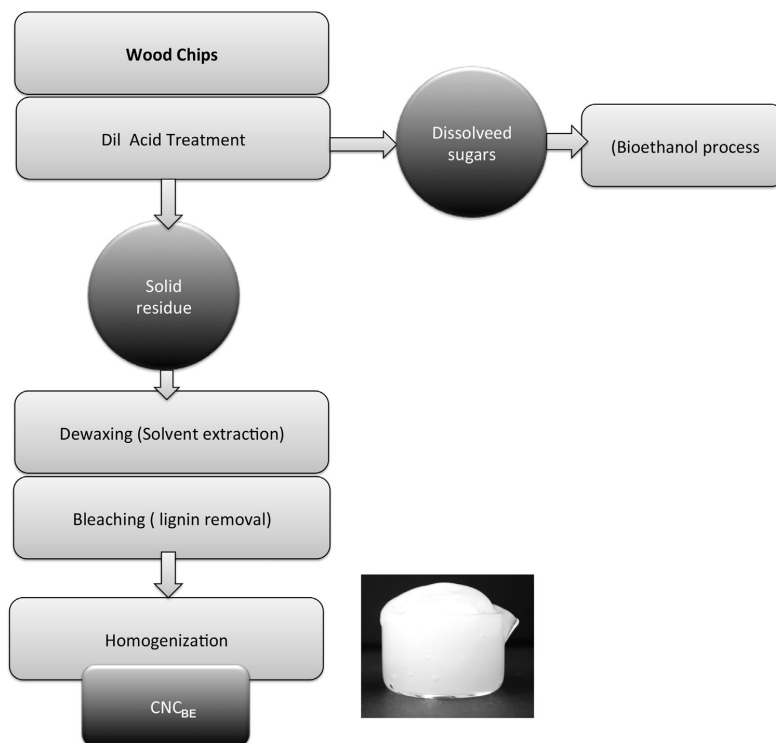


Fig. 1. Schematic representation of the processing of CNC_{BE} and the gel obtained after the process.

of the samples, C 1s and O 1s spectra were measured within first 10 min of exposure. Processing of the spectra was accomplished by Kratos software. High-resolution XPS spectra were fitted using linear combinations of 70:30 Gauss–Lorentzian functions on Shirley background-subtracted spectra. Binding energy (BE) scale was calibrated using aliphatic C 1s component, set at 285.0 eV.

Casted films of CNC were analyzed at the same temperature by step scanning on the Siemens diffractometer D5000 (Berlin, Germany) to understand the crystallinity of the nanomaterials. The angle of incident monochromatic X-ray was in the range of $2\Theta = 10^\circ$ – 30° with a step size of 0.0263. The wavelength of the monochromatic X-ray was 1.540598 Å ($K\alpha 1$). The percentage crystallinity is calculated using Segals equation (Segal et al., 1959).

$$CI(\%) = \frac{I(22^\circ) - I(18^\circ)}{I(22^\circ)} \times 100\% \quad (1)$$

CI(%) in the equation (1) stands for crystalline index of cellulose. $I_{(22^\circ)}$ (arbitrary units) represents the peak diffraction intensity corresponding to crystalline cellulose and $I_{(18^\circ)}$ is the peak diffraction intensity corresponding to the amorphous sections in cellulose, at 22° and 18° respectively.

Tensile tests were performed using strips with dimensions of 5 mm × 50 mm on a universal testing machine, Shimadzu Autograph AG-X (Japan); with a load cell of 1 kN. The gauge length was 20 mm, at a strain rate of 2 mm/min. The elastic modulus was calculated from the initial part of the slope from stress–strain curves. At least five tests were performed for each sample and the average values are presented.

Transparency tests were performed using a UV-visible spectrophotometer (Perkin Elmer, Lambda 2S). CNC films of

approximately 50 × 10 mm were cut and fitted in the sample holder and transmittance was measured over the wavelength region from near ultraviolet (300–400) to visible light (400–800 nm). An empty sample holder was used as a reference. The films were also photographed digitally, against a printed surface to visually observe and compare transparency.

Biocompatibility of CNC and CNF casted films was studied by direct contact test systems. The material was fixed to cell culture dish and the cells (adipose derived stem cells and cell line L929) were seeded evenly throughout the cell culture dish. The impact of the biomaterial on cell growth and morphology was monitored and documented with photographs up to 15 days.

3. Results and discussion

3.1. Isolation process

Fig. 1 shows the scheme of the integration of the CNC_{BE} isolation process with the bioethanol pilot-scale production unit. In the case of bioethanol process after the acid hydrolysis step the liquid fraction of dissolved hemicellulose and amorphous cellulose is collected, where as in the case of CNC_{BE} process, the solid residue stream is collected for further processing. The solid residue obtained was purified to cellulose by bleaching and solvent extraction and thereafter isolated to nanocrystals by a simple mechanical process of homogenization. It may be noted that further acid hydrolysis is not required to obtain CNC_{BE} because it was done at the first step of bioethanol processing. Here the main advantage over starting from pulps or other purified cellulose sources as microcrystalline cellulose is that when acid hydrolysis occurs in

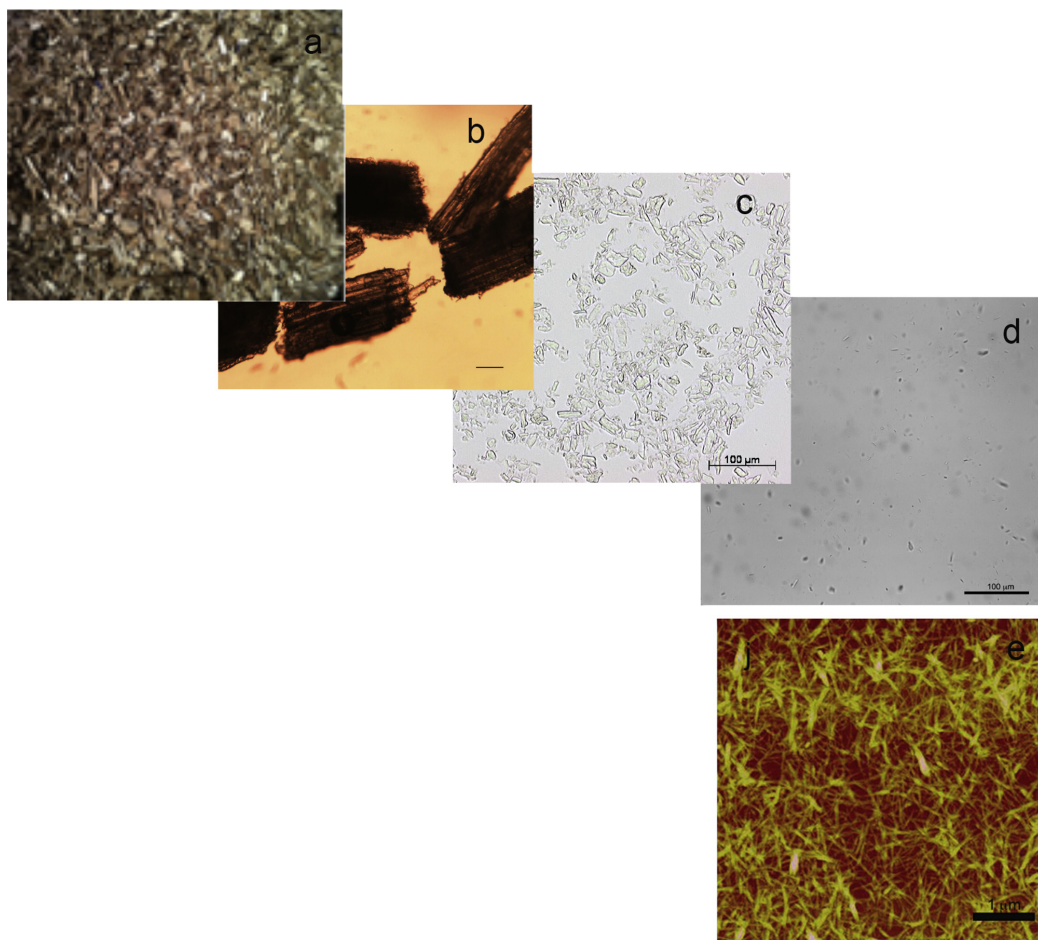


Fig. 2. Images of the studied materials from macro to nanoscale. (a) Photographs of wood chips (b) OM images of wood particles after mild acid hydrolysis (c) OM image after chemical refining (d) OM image after homogenization to nanocrystals and (e) the AFM image of isolated nanocrystals.

the bioethanol pilot-scale unit, the material handled in each step is significantly higher and difficulties related to handling of acids and neutralization in the lab is avoided.

The acid hydrolysis of wood using a bioethanol pilot-scale unit provided materials in large quantities for further processing to cellulose. The yield of the acid hydrolysis step was 46%. After the solvent extraction step to remove extractives, 85% yield was observed and 71–77% yield was recorded after the bleaching step, which removed lignin. This corresponds to 30% pure cellulose with respect to the wood chips at the start. CNC_{BE} isolation by homogenization process resulted in a 100% conversion rate with respect to purified cellulose.

Optical microscopy (OM) and atomic force microscopy (AFM) were used as a tool to study the extent of isolation of the raw material to nanoscaled cellulose and are given in Fig. 2. Figures on the left (Fig. 2a) show the starting materials used. Fig. 2b shows the OM image of the wood particles after the acid hydrolysis step in the pilot-scale facility and OM images of purified wood cellulose (after solvent extraction and bleaching) used for isolating

the nanoparticles are shown in Fig. 2c. Fig. 2d shows the OM of the suspension obtained after the homogenization, where microscaled particles are not visible, indicating that the isolation process has been effective in preparing nanoscaled materials. Atomic force microscopy (AFM) in Fig. 2e gives the nanoscaled information of the isolated materials. The isolated CNC_{BE} had diameters in the range of 5–15 nm. Accurate length determination was not possible from AFM images. The material mostly showed nanocrystal morphology, though some longer nanofibril like structures were also present to a limited extent.

The viscosity of the suspensions increased significantly during mechanical isolation of CNC_{BE} and formed thick gels at low concentrations (see Fig. 1). The viscosity of the CNC_{BE} suspensions at 2 wt% increased from 5 mPa s before grinding to 1440 mPa s after 10 passes through the homogenizer. Gel formation at low concentration is an indication of large surface area, which in turn suggests isolation into nanoscaled structures. CNC_{BE} gels at 2 wt% concentrations showed a semi-transparent nature (see Fig. 1).

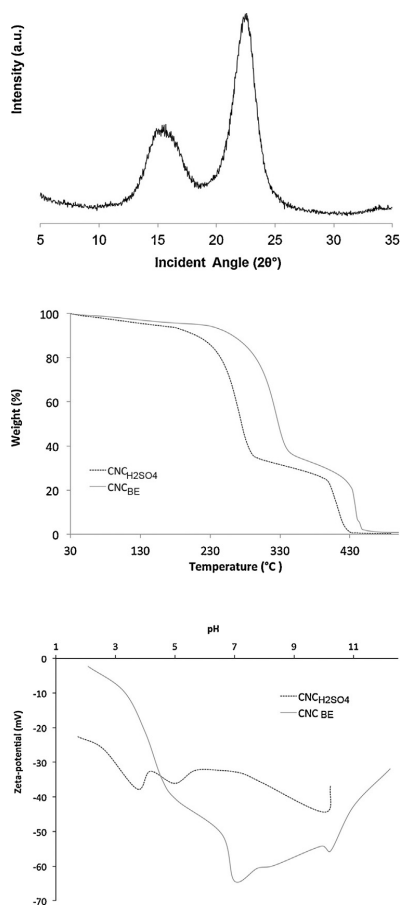


Fig. 3. XRD, TGA and zeta potential data of CNC_{BE}.

3.2. Physical properties

The CNC_{BE} films showed high crystallinity and well defined peaks were visible in the X-ray diffractograms (See Fig. 3a). CNC diffractogram showed peaks at $2\theta = 14.1^\circ$, 16.2° and 22.3° , indicating typical cellulose I structure (Krässig, 1996; Klemm et al., 2005). The percentage crystallinity calculated using Segals's equation from the XRD curves was found to be 77% for CNC. Higher crystallinity of CNC indicates that the process of nanocrystal isolation was efficient to remove amorphous regions. This value is comparable to CNC crystallinity values obtained by acid hydrolysis of MCC (Herrera et al., 2012a; Bondeson et al., 2006).

CNC_{BE} is found to be thermally stable until 240°C (see Fig. 3b) and has higher stability than sulphuric acid hydrolyzed CNC. CNC isolated in the current study by homogenization does not have sulphate groups on the surface that induce the degradation of cellulose and therefore has better thermal stability than traditional acid hydrolyzed nanocrystals. (Roman and Winter, 2004; Bondeson et al., 2006; Herrera et al., 2012a,b).

Zeta potential of the prepared nanomaterial suspensions as a function of pH is shown in Fig. 3c. The zeta potentials of CNC_{BE} remained negative in the studied pH range, which was attributed to negative surface charge, possibly from carboxyl groups. The zeta

Table 1

A comparative study of C 1s and O 1s spectrum of CNC_{SL} and CNC_{BE}.

	CNC _{BE}		H ₂ SO ₄		
	BE, eV	AC, at. %	BE, eV	AC, at. %	
C 1s	285.0	10.62	285.0	24.17	C-(C, H)
	286.6	40.86	286.6	37.2	C-OH
	288.0	9.57	288.1	4.47	O-C-O
	289.2	2.21	289.5	3.45	COOH
O 1s	533.0	35.28	532.0	23.87	

potential was more negative for CNC_{BE} compared to CNC prepared by sulphuric acid hydrolysis in our laboratory (see the dotted lines in Fig. 3c for comparison).

Survey XPS spectra of treated CNC_{BE} and CNC_{H₂SO₄} show different core-level photoelectron peaks attributed to C and O atoms are the main components. Theoretically, pure nanocellulose exhibits two peaks (around 533 and 285 eV) in the full XPS spectra, which correspond to oxygen and carbon, respectively (Siqueira et al., 2010). Both these peaks are present in XPS spectra for CNC_{BE} and CNC_{H₂SO₄} shown in Fig. 4. Table 1 illustrates the introduction of more oxygen at 533 eV in CNC_{BE} compared to CNC_{H₂SO₄} indicating the more oxygen containing moieties on CNC_{BE} surface. Further examination of full XPS spectra of CNC_{H₂SO₄} (Fig. 4b) confirmed the presence of traces of sulfur in the spectrum, S 2p at approximately 165 eV and S 2s at approximately 230 eV (detectable only in detailed analysis and not visible here) and its absence in CNC_{BE}. This indicates the presence of $-\text{SO}_3-$ groups on CNC_{H₂SO₄} as expected. A small amount of Na and F were also detected, which might be impurities.

The main C1s signals for both nanocrystals are decomposed and are shown in the inset. Theoretically, the deconvolution of C1s signal for pure cellulose should exhibit two peaks associated to C-O of alcohols and ethers groups and O-C-O for acetal moieties while in practice the XPS analysis of cellulose always reveals four C peaks: C-C/C-H (C1, 285 eV), C-OH (C2, 286.6 eV), O-C-O (C3, 288.0 eV) and COOH (C4, 289.2 eV) (Siqueira et al., 2010) (see Fig. 4 and Table 1). Both CNC_{BE} and CNC_{H₂SO₄} in Fig. 4 (inset) showed all peaks corresponding to carbon atoms C1, C2, C3 and C4. The magnitude of C2 and C3 peaks is however higher in CNC_{BE}, which indicate the presence of more C-OH and O=C-O on the surface of CNC_{BE} compared to CNC_{H₂SO₄}. The XPS study shows that CNC_{BE} has more surface groups with as carboxyl and carbonyl groups probably introduced during weak acid hydrolysis and the subsequent bleaching steps.

The O=C-O groups on CNC_{BE} can be considered responsible for its negative zeta potential where as SO_3- and O=C-O on CNC_{H₂SO₄} contribute to its negative zeta potential. However, the O=C-O groups on CNC_{BE} is significantly higher (almost double) compared to CNC_{H₂SO₄}, which explains the high negative zeta potential of CNC_{BE}. Our recent studies also showed that negatively charged nanocellulose are capable of preferentially adsorbing positively charged entities as heavy metal ions or dyes from water (Liu et al., 2014; Karim et al., 2014) and therefore CNC_{BE} with high negative zeta potential have potential as functional nanomaterial in water cleaning.

Table 2

Mechanical properties of films and mats of the prepared materials.

Material	Stress (MPa)	Strain (%)	Young Modulus (GPa)
CNC _{BE} (Casting)	204.64 \pm 20.06	2.23 \pm 0.57	16.11 \pm 1.33
CNC _{BE} (Filt and press)	97.58 \pm 8.29	2.47 \pm 0.59	7.25 \pm 1.18

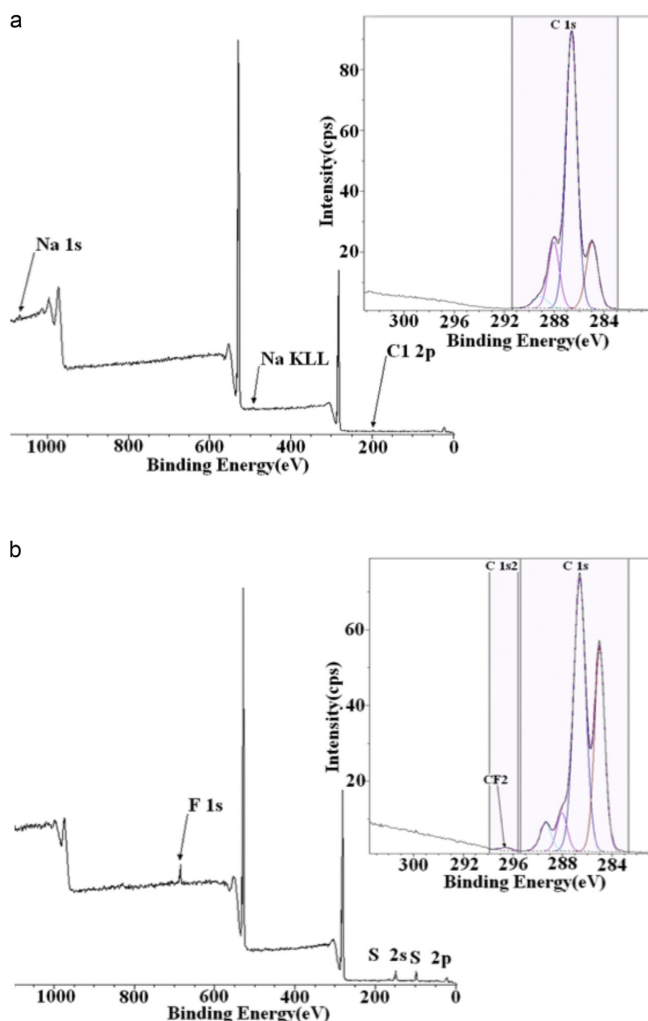


Fig. 4. XPS survey spectra of a) CNC_{BE} and CNCH₂SO₄ and the representative C1s photoemission spectra (inset).

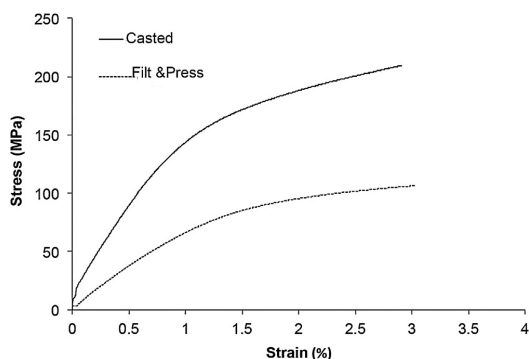


Fig. 5. Stress-strain curves of the films and nanopapers of CNC_{BE}.

3.3. Mechanical properties

Tensile properties of the mats and films prepared from the nano-materials were evaluated to understand the effect of the processing methods on the mechanical properties. The mechanical properties are also considered as an indirect measure of the degree of isolation to nanoscale. The data obtained are given in Table 2 and the stress-strain curves are shown in Fig. 5.

CNC_{BE} showed the best mechanical performance of all the studied materials. The casted films had strength as high as 204 MPa and modulus of 16.11 GPa. The strain at break was similar for CNC_{BE} materials prepared by casting as well as filtration and pressing. The big drop in tensile strength and modulus for the CNC_{BE} prepared by filtration and pressing compared to casted films was unexpected. One possible explanation for the higher mechanical strength for casted films of CNC may be due to less voids, which resulted from slow and organized compacting of nanoparticles during evaporation compared to filtered ones. The tensile data of CNC_{H₂SO₄} are



Fig. 6. Photographs of films of (a) CNC_{BE} (Casting) (b) CNC_{BE} (Filtration & pressing) (c) CNC_{H₂SO₄}, comparing the optical properties.

not presented here, due to the high brittleness of the films which resulted in unreliable values with high standard deviation.

3.4. Optical properties

The optical properties of the CNC_{BE} films (Fig. 6a) and mats (Fig. 6b) are shown in Fig. 6 and were compared with CNC_{H₂SO₄} (Fig. 6c). All the films showed transparency, but the highest transparency was observed for CNC_{H₂SO₄}. UV-visual data at 540 nm, showed 58% transparency for CNC_{H₂SO₄}, while it decreased to the range of 16 and 12%, respectively, for CNC_{BE} casted and CNC filtered and pressed (curves not shown). The reason for lower transparency for CNC from bioethanol process was attributed to nanocrystals with lengths higher than wavelength of light (Herrera et al., 2012b). It was also noted that casting resulted in films with better

transparency than filtration and pressing, even though the differences were minimal. The higher transparency for casted films may be due to less voids and compacted films and is in agreement with the mechanical data discussed in Section 3.3. However, in general, the transparency values obtained are lower than those found in some earlier reports for nanocellulose (Herrera et al., 2012b; Uetani and Yano, 2011).

3.5. Cytocompatibility

Fig. 7 shows the cell adhesion and growth of primary human cells and L929 on negative control and CNC_{BE}. The films surfaces of CNC_{BE} showed the growth of cells after 15 days of incubation indicating its non-toxic and cytocompatible nature. The study shows

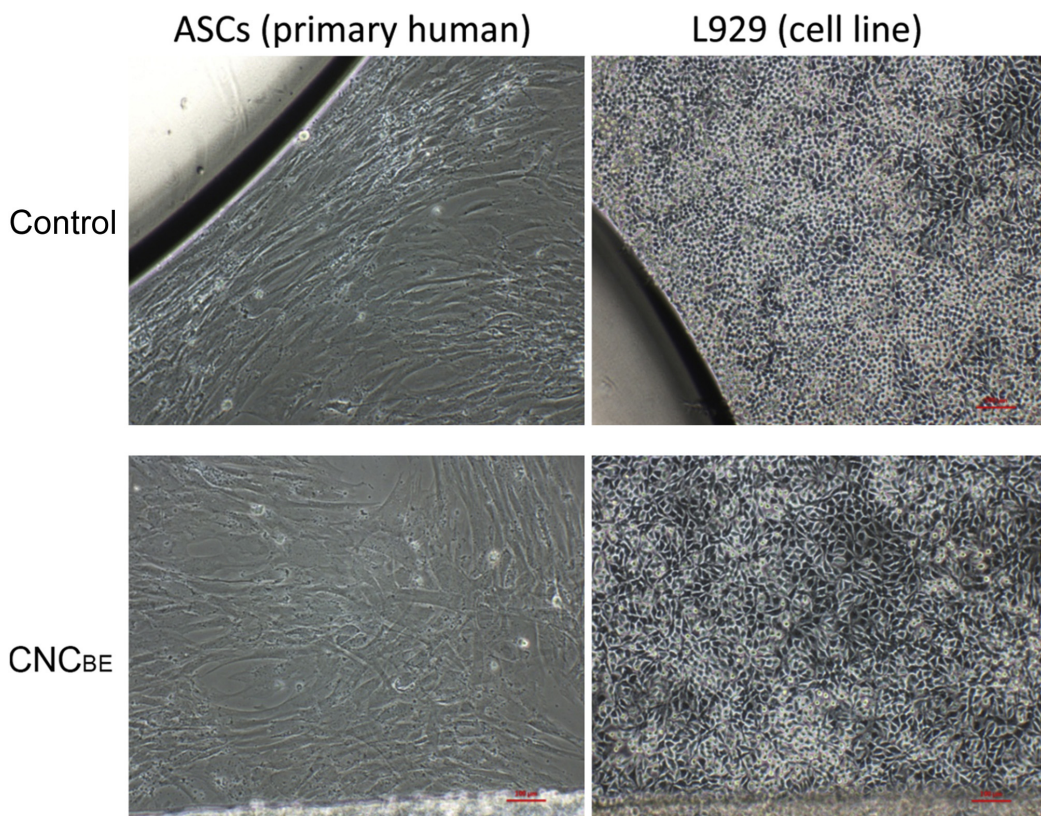


Fig. 7. Images showing adhesion and growth of primary human cells and L929 cells on the negative control and films of CNC_{BE} after 15 days of incubation.

the potential of CNC_{BE} in biomedical products and implants where cell viability is crucial.

3.6. Process efficiency

The adopted processing route resulted in scaled-up production of CNC in the lab. The processing route achieved CNC_{BE} yield in the range of 600 g/day (excluding the pilot-scale acid hydrolysis process and the cellulose refining step), which is a major improvement compared to 50 g/week in lab-scale processing.

The energy consumption for the mechanical isolation step at laboratory scale was estimated to be 30 kWh/kg for CNC_{BE}. The total energy consumption for the scaled-up process including industrial/pilot-scale steps is not discussed here and will be reported in detail separately.

4. Conclusions

The isolation of cellulose nanocrystals from wood chips via bioethanol pilot-scale unit resulted in CNC_{BE} processing in the range of 600 g/day.

CNC_{BE} produced by the scaled-up processes had cellulose I structure and negative zeta potential being related to the surface groups providing interactions with positively charged entities. The CNC_{BE} films had mechanical strength as high as 204 MPa and modulus of 16 GPa, showing their potential as nanoreinforcement. The nanocrystals were also found to be cytocompatible towards primary human cells and L929 cells indicating potential in biomedical applications.

The new process route developed can be adopted easily by research laboratories and small-scale industries to produce nanocrystals in larger scale at the point of use, via mechanical isolation of cellulose from bioethanol production.

Acknowledgments

Financial support from the European Commission under EU FP7, NMP4-SL-2012-280519, NanoSelect is gratefully acknowledged. The authors wish to thank Dr. Anuttam Patra, Department of Civil, Environmental and Natural Resources Engineering, LTU, Sweden for help with UV/Visual measurements. Mirjam Fröhlich and Lenart Girando, EDUCELL, Slovenia is acknowledged for biocompatibility data. Processum Biorefineries, More Research and SEKAB E-technologies Örnsköldsvik Sweden are gratefully acknowledged for providing raw materials and cellulose purification.

References

- Bondeson, D., Mathew, A.P., Oksman, K., 2006. Optimization of the isolation of nanocrystals from microcrystalline cellulose by acid hydrolysis. *Cellulose* 13, 171–180.

- Chauve, G., Bras, J., 2014. Industrial point of view of nanocellulose materials and their possible applications, Ch 14, In *Handbook of Green Materials, Processing Technologies, Properties and Applications*. Vol 1, K Oksman, A. Mathew, M. Sain, A Bismarck and O Rojas, (Eds). World Scientific ISBN: 978-981-4566-45-2 pp. 234–252.
- Dufresne, A., 2008. Cellulose-based composites and nanocomposites, In *Monomers, Polymers and Composites from Renewable Resources*, Elsevier, pp. 401–418.
- Edgar, C.D., Gray, D.G., 2003. Smooth model cellulose I surfaces from nanocrystals suspensions. *Cellulose* 10, 299–306.
- Eichhorn, S., Dufresne, A., Aranguren, M., Marcovich, N., Capadona, J., Rowan, S., Weder, C., Thielemans, W., Roman, M., Renneckar, S., Gindl, W., Veigel, S., Keckes, J., Yano, H., Abe, K., Nogi, M., Nakagaito, A., Mangalam, A., Simonsen, J., Benight, A., Bismarck, A., Berglund, L., Peijs, T., 2010. Review: Current international research into cellulose nanofibres and nanocomposites. *J. Mater. Sci.* 45, 1–33.
- FutureMarkets, Inc., Market Study—Nanocellulose: a technology and market study—Version 2 (2012). http://www.futuremarketsinc.com/index.php?option=com_content&view=article&id=206&Itemid=82
- Han, J.S., Rowell, J.S., 1996. Chemical composition of fibers. In: Rowell, R.M., Young, R.A., Rowell, J. (Eds.), *Paper and Composites from Agrobased Resources*. CRC Press, London.
- Herrera, M.A., Mathew, A.P., Oksman, K., 2012a. Comparison of cellulose nanowhiskers extracted from industrial bio-residue and commercial microcrystalline cellulose. *Mater. Lett.* 71, 28–31.
- Herrera, M.A., Mathew, A.P., Oksman, K., 2012. Characterization of cellulose nanowhiskers: A comparison of two industrial bio-residues. *Mater. Sci. Eng.* 31, 012006.
- Hon, D.N.S., ed, 1996. Chemical Modification of Lignocellulosic Material, Marcel Dekker Inc., New York, pp. 11–17.
- Jonoobi, M., Mathew, A.P., Oksman, K., 2012. Producing low-cost cellulose nanofiber from sludge as new source of raw materials. *Ind. Crops Prod.* 232–238.
- Karim, Z., Mathew, A.P., Oksman, K., Grahn, M., Mouzon, J., 2014. Nanoporous membranes containing cellulose nanocrystals as functional additive: Evaluation of removal of dyes from water. *Carbohydrate Polymers*. (submitted).
- Krässig, H.A., 1996. Cellulose: Structure, Accessibility and Reactivity. Volume 11. (Netherlands, Gordon and Breach Science Publisher). Chapter 4.
- Klemm, D., Heublein, B., Fink, H.P., Bohn, A., 2005. Cellulose: fascinating biopolymer and sustainable raw material. *Angew. Chem. Int. Ed. Engl.* 44 (22), 3358–3393.
- Liu, P., Sehaqui, H., Tingaut, P., Wichser, A., Oksman, K., Mathew, A.P., 2014. Biobased nanomaterials for capturing silver ions (Ag⁺) from water via surface adsorption. *Cellulose* 21, 449–461.
- Oksman, K., Etang, J.A., Mathew, A.P., Jonoobi, M., 2011. Cellulose nanowhiskers separated from a bio-residue from wood bioethanol production. *Biomass Bioenergy* 35, 146–152.
- Marchessault, R.H., 1959. Liquid crystal systems from fibrillar polysaccharides. *Nature* 184, 632–633.
- Mathew, A.P., Laborie, M.G., Oksman, K., 2009. Cross-Linked chitosan/chitin crystal nanocomposites with improved permeation selectivity and pH stability. *Biomacromolecules* 10, 1627–1632.
- Roman, M., Winter, W., 2004. Effect of sulfate groups from sulfuric acid hydrolysis on the thermal degradation behavior of bacterial cellulose. *Biomacromolecules* 5, 1671–1677.
- Rånby, B.G., 1952. The cellulose micelles. *TAPPI* 35 (2), 53–58.
- Samir, M.A.S.A., Alloin, F., Dufresne, A., 2005. Review of recent research into cellulosic whiskers, their properties and their application in nanocomposite field. *Biomacromolecules* 6, 612–626.
- Segal, L., Greely, J.J., Martin, A.E., Conrad, C.M., 1959. An empirical method for estimating the degree of crystallinity of native cellulose using x-ray diffractometer. *Text. Res. J.* 29:786–794.
- Siro, I., Plackett, D., 2010. Microfibrillated cellulose and new nanocomposite materials. A review. *Cellulose* 17, 459–494.
- Siqueira, G., Bras, J., Dufresne, A., 2010. New process of chemical grafting of cellulose nanoparticles with a long chain isocyanate. *Langmuir* 26, 402–411.
- Uetani, K., Yano, H., 2011. Nanofibrillation of wood pulp using a high-speed blender. *Biomacromolecules* 12 (2), 348–353.

Paper B



Nanoporous membranes with cellulose nanocrystals as functional entity in chitosan: Removal of dyes from water



Zoheb Karim^{a,b}, Aji P. Mathew^{a,*}, Mattias Grahn^b, Johanne Mouzon^b, Kristiina Oksman^a

^a Division of Materials Science, Luleå University of Technology, 97187, Luleå, Sweden

^b Department of Civil, Environmental and Natural Resources Engineering, Division of Sustainable Process Engineering, 97187, Luleå, Sweden

ARTICLE INFO

Article history:

Received 19 April 2014

Received in revised form 7 June 2014

Accepted 11 June 2014

Available online 25 June 2014

Keywords:

Cellulose nanocrystals

Chitosan

Nanoenabled membranes

Dye removal

Water purification

Adsorption

ABSTRACT

Fully biobased composite membranes for water purification were fabricated with cellulose nanocrystals (CNCs) as functional entities in chitosan matrix via freeze-drying process followed by compacting. The chitosan (10 wt%) bound the CNCs in a stable and nanoporous membrane structure with thickness of 250–270 μm , which was further stabilized by cross-linking with glutaraldehyde vapors. Scanning electron microscopy (SEM) studies revealed well-individualized CNCs embedded in a matrix of chitosan. Brunauer, Emmett and Teller (BET) measurements showed that the membranes were nanoporous with pores in the range of 13–10 nm. In spite of the low water flux ($64 \text{ L m}^{-2} \text{ h}^{-1}$), the membranes successfully removed 98%, 84% and 70% respectively of positively charged dyes like Victoria Blue 2B, Methyl Violet 2B and Rhodamine 6G, after a contact time of 24 h. The removal of dyes was expected to be driven by the electrostatic attraction between negatively charged CNCs and the positively charged dyes.

© 2014 Elsevier Ltd. All rights reserved.

1. Introduction

Shortage and contamination of global drinking water call for the development of highly effective water purification techniques. The removal of various pollutants such as heavy metals, dyes, pesticides, herbicides and other industrial as well as agricultural wastes from wastewater has become a critical issue due to their adverse effects on human health and environment (Huang, Chang, Ou, Chiang, & Wang, 2011; Lin, Chen, Chien, Chiou, & Liu, 2011).

Recently, advances in nanoscale science and engineering suggest that many of the current problems involving water quality could be greatly diminished by using nanomaterials due to their good adsorption efficiency, higher surface area and greater active sites for interaction with pollutants (Dhermendra, Behari, & Prasenjit, 2008; Diallo, Christie, Swaminathan, Johnson, & Goddard, 2005). Several studies have shown the effectiveness of nano-enabled membranes for cleaning industrial wastewater such as fish-meal wastewater, solutes from etching processes, wastewater from textile industry, etc. (Dhermendra et al., 2008; Ma, Burger, Hsiao, & Chu, 2011a). However these technologies poses significant challenges in term of limited availability of nanomaterials, cost effectiveness and environmental concerns.

Polysaccharides, such as cellulose and chitin, are among the most abundant biomaterials on earth, having low cost, environmental friendly, renewable and biodegradable properties (Muzzarelli, 2012; Muzzarelli et al., 2007; Samir, Alloin, & Dufresne, 2005). By intelligent processing techniques and properties they could be used as classical nano-reinforcements/functional elements in polymers for the preparation of membranes (Ma et al., 2011a; Ma, Burger, Hsiao, & Chu, 2012). Cellulose nanocrystals (CNCs) and nanofibers isolated from bioresources have been studied as reinforcements and/or functional entity in various synthetic and natural polymer matrices and for different applications (Kvein et al., 2007; Mathew, Oksman, Pierron, & Harmand, 2012; Mikkonen et al., 2010; Narges et al., 2014; Petersson, Kvein, & Oksman, 2007; Samir et al., 2005; Saxena, Elder, Pan, & Ragauskas, 2009). Recently, Ma et al. (2012) developed a membrane, where ultrafine CNCs were infused into an electrospun polyacrylonitrile nanofibrous scaffold supported by mechanically strong polyethylene terephthalate non-woven substrate. The impregnated CNCs possessed very high negative surface charge density and thus provided high adsorption capacity to remove positively charged species, viz. crystal violet dye. Thus, adsorption has been proved to be an economical method for the treatment of wastewater contaminants. Now-a-days, almost all the adsorbents developed for removal of contaminants rely on the surface interactions and therefore the functional groups available on the surface of the adsorbents played an important role in determining the effectiveness, capacity,

* Corresponding author. Tel.: +46 92493336.

E-mail address: aji.mathew@ltu.se (A.P. Mathew).

selectivity and reusability of the adsorbent material (Dural, Cavas, Papageorgiou, & Katsaros, 2011; Liu, Wang, & Li, 2005; Wesenberg, Kyriakides, & Agathos, 2003; Xiao et al., 2010). Furthermore large surface area and abundance of adsorption sites are essential for adsorption and removal of the contaminants from wastewater (Li & Bai, 2005; Li, Bai, & Liu, 2005; Liu et al., 2014).

In the current study CNCs having required functional groups (SO_3^- and/or COO^-) (Liu et al., 2014) for the removal of targeted dyes by electrostatic interaction, are used as functional entity for the fabrication of composite membranes. Chitosan is used as the matrix phase. Though chitosan is traditionally used in water purification, it is mostly effective toward negatively charged acidic dyes due to functional group present on chitosan ($-\text{NH}_2^+$) (Bingjie, Dongfeng, Guangli, & Xianghong, 2013; Crini, 2006). However, the water permeability and water stability of chitosan in different pH conditions, especially after cross-linking will be of advantage in fabricating water-cleaning membranes (Mathew, Laborie, & Oksman, 2009). A very simple technique, freeze-drying was applied for the fabrication of composite membranes. The biggest advantage with process was fabrication of a loose and non-aggregated network, which is expected to provide easy availability of surface groups on CNCs as adsorption sites for contaminants. High concentration of functional entity (CNCs) was used with an aim to have high process efficiency. The process method as well the matrix used is expected to make the surfaces of functional entity readily available for interaction with contaminants in water.

ATR-FTIR analysis was performed to understand the basic binding parameters with CNCs and matrix, chitosan. SEM and BET techniques were used to characterize the membrane morphology and pore structure. Flux and mechanical performance of the composite membranes were also determined. Three positively charged dyes (Victoria Blue 2B, Methyl Violet 2B and Rhodamine 6G) that are real concern in industrial wastewater were chosen for the study. It may be noted that these dyes are of industrial and environmental relevance as (i) according to the Swedish Environmental Protection Agency, the selected dyes came under section “very hazardous” contaminants, (ii) the three selected dyes having negative impact in southern Europe, especially in Spain and (iii) these dyes had very harmful effects not only on human but on aquatic life also.

2. Experimental

2.1. Materials

Non-dried cellulose residue (sludge) from dissolving cellulose production was obtained from Domsoj Fabriker AB, Ornskoldsvik Mill, Sweden, with a water content of 50 wt%. Based on the data from the material supplier, the chemical composition of the used sludge was, cellulose content (95%), hemicellulose (4.75%) and very low content of lignin.

Chitosan from shrimp shells (medium molecular weight having deacetylation value $\geq 75.5\%$ and viscosity, 20–300 cps), polyethylene glycol (PEG 2000) and glutaraldehyde (50%) were purchased from Sigma–Aldrich (USA). Acetic acid (96%) and sulfuric acid (98%) were supplied by VWR (BDH, France).

Sludge was used as received without any pretreatments and all chemicals were used without any purification.

2.2. Processing methods

2.2.1. Isolation and characterization of CNCs

CNCs were prepared by acid hydrolysis of non-dried cellulose residue (sludge) following the sulfuric acid hydrolysis as procedure by Bondeson, Mathew, and Oksman (2006), with minor modifications. The sludge was hydrolyzed with 63.5% sulfuric acid for

105 min at 45 °C. The resulting suspension underwent a series of centrifugation, washing with deionized water, and sonication steps to collect the CNCs in the supernatant. This was neutralized by dialysis and stored until further use in the form of aqueous suspensions. Isolated CNCs were concentrated by dialysis against PEG to a concentration of 4.2 wt% prior to use for membrane fabrication. The yield of CNCs from the process was 17% with respect to the used cellulose residue weight.

2.2.2. Preparation and cross-linking of nanocomposite membrane

Chitosan was first dissolved in 2 wt% acetic acid followed by addition of deionized water to form a solution of 1 wt%. The concentrated CNCs were mixed with chitosan solution in 9:1 ratios and the total concentration of mix was 2 wt%. The mixture of chitosan and CNCs were casted into Petri plates and put into freezer to solidify. The solidified mixture was freeze-dried in an ALPHA 2–4 LD Plus freeze dryer at -75°C for 24 h. After freeze-drying, the prepared porous composites were pressed between aluminum plates in a compression molding machine (Fontune Presses, Elastocon, Sweden) without heating to obtain compacted membranes. Same procedure was followed for the preparation of native chitosan (0.2 wt%), used as control. Cross-linking was performed by placing the compacted membranes in a desiccator with glutaraldehyde vapors; 25% of glutaraldehyde at room temperature for 48 h was used. In uncross-linked as well as cross-linked membranes the final CNC concentration was 90 wt%.

2.3. Characterizations

2.3.1. Morphology and pore structure

Atomic force microscopy (AFM) was analyzed using a Veeco Multi Mode instrument equipped with Nanoscope V controller. A droplet of the aqueous CNCs suspension (0.2%) was dried on a freshly cleaved mica surface prior to AFM examination. AFM images were captured in tapping mode using coated Si probes at a resonance frequency of 70 kHz and having a spring constant of 1–5 N/m.

The morphology of uncross-linked and cross-linked membranes was examined at high magnification using MAGELLAN 400, SEM (FEI Company). The membranes were fractured and sputter coated with tungsten. The films were observed in the SEM at an acceleration voltage of 20 kV.

2.3.2. Chemical characteristics

A Bruker IFS 66v/S spectrometer equipped with liquid nitrogen cooled mercury–cadmium–telluride (MCT) detector and a vertical ATR-FTIR accessory was used for collecting infrared data. Both single beam background and sample spectra were acquired by averaging 500 scans at a resolution of 4 cm^{-1} . Spectra evaluation was performed using the Bruker Opus 4.2 software.

2.3.3. Porosity

Specific surface area and pore size of fabricated composites were determined by N_2 adsorption using BET method with sample-degassed instrument (Micromeritics ASAP 2000, Sweden) at 100°C for 24 h in dry N_2 flow.

2.3.4. Mechanical properties

The tensile tests of the uncross-linked and cross-linked membranes were performed using a universal testing machine, Shimadzu Autograph AG-X (Japan), with a load cell 1 kN and the gauge length was 20 mm. Test specimens were 5 mm and 0.25 mm in nominal width and thickness as measured by digital caliper for membrane. The samples were preloaded with 1 N before starting the tensile test. The samples were stretched with 2 mm/min crosshead speed until failure. The stress–strain curves were plotted from the measured load and samples extension. The stress is

defined as $\sigma = F/(A_0 L_0)$ and the strain as $\varepsilon = \ln(L/L_0)$, where F is the instantaneous force, A_0 is the initial sample cross section, and L_0 is the initial sample length. The elastic modulus was calculated from the initial part of the slope from the stress–strain curve. At least five test samples were tested for each material and the average values were presented.

2.3.5. Flux measurement

A dead-end stirred cell filtration system connected with a N_2 gas cylinder was used to evaluate the flux performance of the composite membranes. All experiments were carried out using a filtration test cell, Dead End Cell (Sterlitech HP4750 Stirred cell, USA) with a capacity of 300 ml. The effective area of the membrane was 17.3 cm^2 . The operation pressure (0.196 MPa) in the system was maintained by nitrogen gas. Composite membranes were conditioned in water for 1 day prior to measurement of water flux. The amount of solvent passing through the membranes under applied pressure within a fixed time interval was used to calculate water flux ($\text{L m}^{-2} \text{ h}^{-1} \text{ MPa}^{-1}$). The water flux (F) was calculated using Eq. (1).

$$F = \frac{V_0 (\text{L})}{T_0 (\text{h})} \times A_0 (\text{m}^2) \times P_0 (\text{MPa}) \quad (1)$$

where V_0 is the volume of solvent that passed through the membrane, T_0 is the time of measurement, A_0 is the effective membrane area and P_0 is the applied pressure.

It was not possible to measure the water flux of pure chitosan as the freeze-dried structure was completely destroyed because of

dipping chitosan membrane in water before measurement of water flux.

2.3.6. Evaluation of dye removal efficiency

The quantitative analysis of untreated and treated model wastewater was determined by UV–vis spectrophotometer (Perkin Elmer, Lambda 2S, Sweden). The percentage removal was calculated by the formula given below:

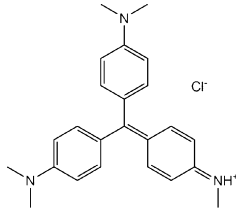
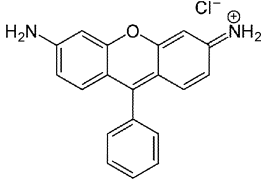
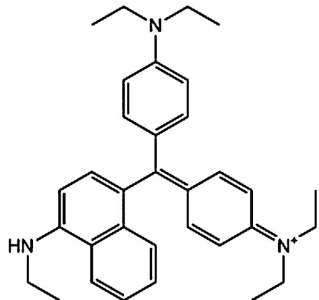
$$A_0 - \frac{A_t}{A_0} \times 100 \quad (2)$$

where A_0 is the absorbance of treated dye solution with chitosan membrane and A_t is the absorbance of treated dye solution with composite membrane. The absorbance of each dye was recorded at their λ_{max} , determined by UV–vis spectrophotometer. The optical absorbance of dyes, Methyl Violet 2B, Rhodamine 6G and Victoria Blue 2B at 581, 526 and 616 nm respectively was monitored by UV–vis spectroscopy to determine the percentage removal of dyes. Table 1 summarizes the chemical structure and other parameters of the used dyes.

Some screening experiments on the effect of pH, incubation time and doses of dyes with uncross-linked hybrid membrane only, were performed to determine the best conditions to study the maximum removal efficiency of the prepared hybrid membranes.

Stock solution of model wastewater was prepared by adding dyes (10 mg/L) in deionized water. The 1 mg/L of model wastewater was used with uncross-linked and cross-linked membranes. Composite membranes cut into $30 \times 20 \text{ mm}$ of pieces were incubated for 24 h in solution of pH 5.01 at room temperature (23 ± 2) with

Table 1
Information about targeted dyes.

Name of dyes	Core structure of dyes	Nomenclature in text	λ_{max}	Charge on surface
Methyl Violet 2B		MV 2B	581 nm	+
Rhodamine 6G		R6G	526 nm	+
Victoria Blue 2B		VB 2B	616 nm	+

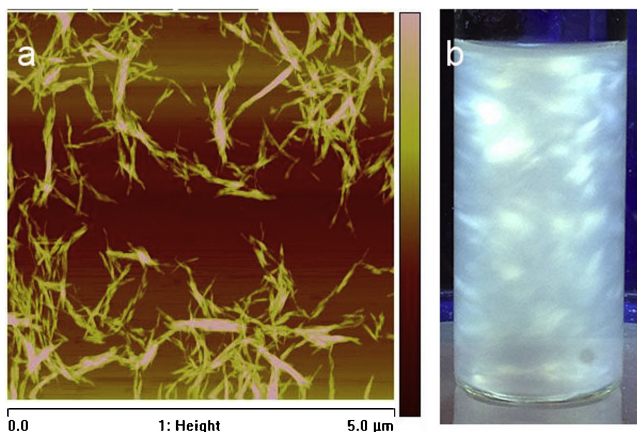


Fig. 1. (a) AFM image of isolated CNCs and (b) flow birefringence of CNCs suspension, observed between two crossed polarizers.

stirring. The model wastewater treated with 0.2% chitosan was taken as control for determination of percentage removal by composite membranes using formula mentioned above. All experiments were performed in dark to prevent the photo-degradation.

3. Results and discussion

3.1. Characteristics of cellulose nanocrystals

The AFM images in Fig. 1 show the presence of isolated cellulose nanocrystals in the nanometer scale. CNC displays rod-like shape with diameters in the range of 6–10 nm, as measured by Nanoscope V software. The nanocrystal dimension agrees with our earlier reports of CNC prepared with same isolation process, by Kvien, Tanem, and Oksman (2005) to be of 5 ± 2 nm width and length of 210 ± 75 nm. The flow birefringence (Fig. 1b) of aqueous nanocrystals when viewed under cross-polarized light also supported the existence of CNCs (Araki, Wada, Kuga, & Okani, 2000; Bondeson et al., 2006).

Crystallinity of isolated CNCs was 70%, and had a surface charge density of $230 \mu\text{mol/g}$ as calculated from the conductometric titration curve. The Z-potential of CNCs remained negative in the pH range of 3–12, as reported in our previous published work (Liu et al., 2014).

3.2. Morphology of prepared composite membrane

Fig. 2a and c shows the overview images for uncross-linked and cross-linked nanocomposite membranes, respectively. The thickness of the membrane was estimated to be in the range of $250\text{--}270 \mu\text{m}$. In both cases layered structure was observed, which is expected to have formed during compacting of freeze-dried material. Another reason is the high concentration of used CNCs. Recently, Han et al. (2013) reported the concentration dependent mechanism for lamellar or fiber structure morphology of nanocellulose through freeze-drying. According to their results, at low concentration (0.05 wt%), nanocelluloses were self-assembled into oriented ultrafine fibers but at high concentration (0.5 and 1 wt%), the lamellar structured foam composed of aligned thin membrane layers. Similar layered structures were reported for freeze-dried membranes from nanocellulose fibers also (Gebald, Wurzbacher, Tingaut, Zimmermann, & Steinfeld, 2011). The images also show that the cross-linked system is slightly denser than the uncross-linked ones.

Fig. 2b and d shows the detailed view of the uncross-linked and cross-linked nanocomposite membranes. The detailed image shows the nanoscaled morphology of the membranes while the inset image shows one layer of the membranes. The SEM images of uncross-linked membranes showed that CNCs were regularly dispersed within the chitosan network of CNCs with absence of visible agglomerates (Fig. 2b). Cross-linked nanocomposite membrane also shows uniform dispersion of CNCs within the chitosan network in random orientation but little tight network due to the cross-linking with glutaraldehyde (Fig. 2d). The good dispersion of CNCs in chitosan matrix even at high concentration indicates positive interaction between chitosan matrix and CNCs. It may be considered that the CNCs are bound together in a three dimensional network by chitosan chains. In the current study also we have the advantage of the common solvent and furthermore the processing methods used, viz. freeze-drying is considered as an efficient route to limit aggregation of nanocellulose.

Gebald et al. (2011) recently reported cellulose nanofibers membrane for the adsorption of CO_2 prepared by freeze-drying. In this study, SEM images of prepared membrane revealed single irregularly distributed cellulose fibrils attached to the cellulose sheet, after freeze-drying and aggregation of cellulose nanofibrils to form sheet upon freezing was recorded. It is expected that in the current study the combination of the choice of matrix, and the processing method have positively impacted the homogeneous dispersion and distribution of CNCs. The infused and well-dispersed CNCs within the chitosan network offer several advantages in membrane technology as high surface-to-volume ratio that makes them high adsorption efficiency toward contaminants.

3.3. Evaluation of molecular level interactions

To understand the interaction between the chitosan polymer and CNCs in the composite membrane, FTIR spectroscopy of the samples was performed using the ATR (attenuated total reflection) technique (see supplementary data for the spectrum). The spectra of chitosan and CNCs were typical to spectra previously reported on these substances (Pavia, Lampman, & Kriz, 2002). The main bands in the spectrum of chitosan were located around 1643 and 1558 cm^{-1} . The first band was for C=O stretching of acetyl group and the second band was the N-H bending vibrations of amide and amine groups. The bands at 1070 cm^{-1} and 1030 cm^{-1} were due to the C-O stretching vibration, whereas the broad band at $3100\text{--}3400 \text{ cm}^{-1}$ was on behalf of O-H and N-H stretching

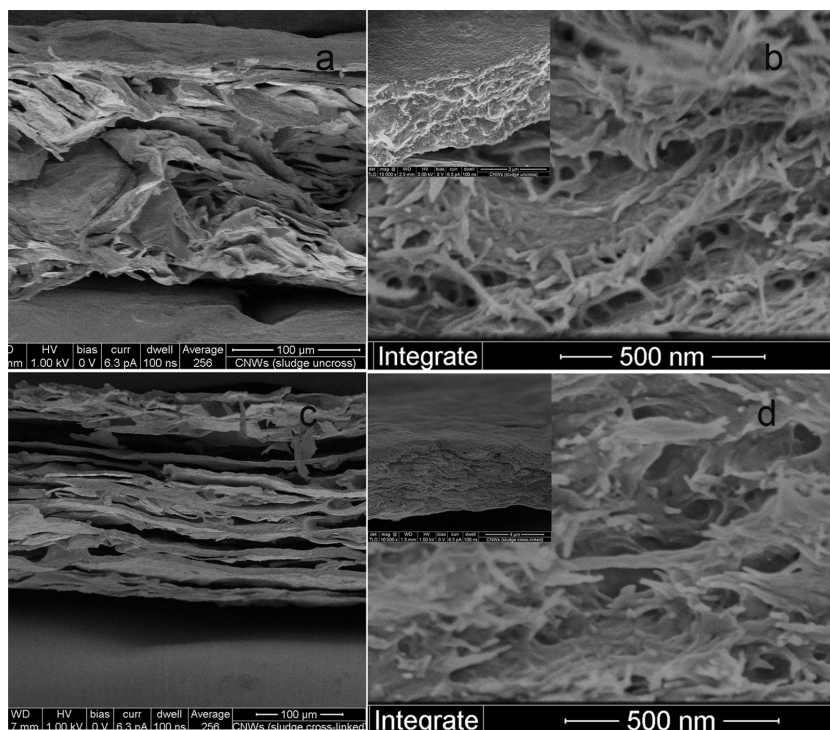


Fig. 2. SEM images of prepared membranes showing (a) layered structure of uncross-linked membranes; (b) the detailed view of the membrane showing the homogeneous dispersion of CNCs in the matrix; c) the layered structure of cross-linked membranes; (d) the detailed view of the CNCs dispersed in the cross-linked matrix. In inset images show one layer of the uncross-linked membrane (inset b) and cross-linked membrane (inset d), comparing the compactness before and after cross-linking.

vibrations. The peaks 1375 cm^{-1} and 1350 cm^{-1} were indicating $-\text{CH}_3$ group of *N*-acetyl glucosamine residue and $-\text{CH}_2$ groups, respectively. All mentioned peaks were in the agreement of previous reported works. (Brown, Laborie, & Zhang, 2011; Shigemasa, Matsuura, Sashiwa, & Saimoto, 1996).

In pure CNCs, the broad band centered at $\text{ca } 3400\text{ cm}^{-1}$ was related to $\text{O}-\text{H}$ stretching vibration. The bands at 2893 cm^{-1} and 1431 cm^{-1} were characteristic of $\text{C}-\text{H}$ stretching and bending of $-\text{CH}_2$ groups, respectively, where the peaks at 1160 cm^{-1} and 1070 cm^{-1} were typical to the saccharide structure as mentioned and summarized by Strand, Sauperl, and Fras-Zemljic (2010).

The spectrum of nanocomposite membrane shows characteristic bands of both raw materials (CNCs and chitosan). The saccharide and the $\text{C}-\text{H}$ stretching bands at 1160 cm^{-1} and 1070 cm^{-1} in CNC could be observed in the spectrum of the nanocomposite membrane as well as bands related chitosan viz. the $\text{C}=\text{O}$ stretching and $\text{N}-\text{H}$ bending bands at 1643 cm^{-1} and 1558 cm^{-1} , respectively. Given the structure of chitosan and CNCs and the processing method used, the formation of hydrogen bonds between these compounds is less expected. Both electrostatic and dispersion forces may however also play a part in keeping the composite membranes together. In the case of cross-linked nanocomposite membrane, a relatively weak characteristic absorption band $1550\text{--}1600\text{ cm}^{-1}$ can be assigned to the Schiff base (Brown et al., 2011).

It is expected that similarities between the chemical and molecular structures of CNCs and chitosan enable high affinity between both polymers. Generally, CNCs–chitosan intermolecular interaction are based on H-bond, van der Waals forces, ionic and/or covalent bonds, depending on the processing route (Al-Ghouti et al.,

2010). In this study, the process of hybrid membrane fabrication was freeze-drying which was directly responsible for the absence of hydrogen bonding, resulting loose network between CNCs and matrix, chitosan. Thus, the bonding between functional entity, CNCs and matrix, chitosan was predominantly by electrostatic interaction, dispersive forces and chemical bonds. The isolation of CNCs with acid hydrolysis (H_2SO_4) introduced sulfate groups (replaced by aldehyde) onto the surface of CNCs. So there was a high chance for introduction of electrostatic interaction within the CNCs and chitosan. According to Strand et al. (2010), the binding of cellulose on chitosan depends only on two factors; (i) a satisfactory amount of anchoring sites especially, introduction of functional groups in/on cellulose, onto which chitosan could bind and at the same time (ii) satisfactory free amino groups of chitosan, and both these binding mechanisms are applicable in the current system.

3.4. Measurement of pore size and surface area of composite membrane

The BET results were summarized in Table 2. The BET surface areas of uncross-linked and cross-linked composite membranes

Table 2
BET results of uncross-linked and cross-linked membranes.

Type	BET surface area (m^2/g)	Average pore size (nm)
Uncross-linked membrane	3.1	17
Cross-linked membrane	2.9	13

Table 3

Mechanical testing results of uncross-linked and cross-linked composite membranes.

Types of membranes	Max stress (MPa)	Strain at break (%)	Modulus of elasticity (MPa)
Uncross-linked	0.98 ± 0.4	0.28 ± 0.4	128 ± 0.6
Cross-linked	1.1 ± 0.3	0.23 ± 0.5	318 ± 0.4

were 3.1 and 2.9 m²/g, respectively. This surface area is lower than some earlier reports on freeze-dried nanocellulose membrane structures. The freeze-dried NFC showed a BET surface area of 26.8 m²/g whereas the amine functionalized NFC showed 7.1 m²/g (Gebald et al., 2011). In the current freeze-dried structures, the compacting process was considered to be responsible for the relatively lower surface area, recorded in BET measurements. The pore sizes of membranes were also determined by same technique and were found to be 17 and 13 nm for uncross-linked and cross-linked composite films, respectively. From these results it was confirmed that the cross-linking decreases surface area as well as pore size of nano-enabled membrane and thereby can be considered as more compacted than the uncross-linked one. This data also supports the SEM observations. The decrease of pore size was also reported by Gebald et al. (2011) when amine was loaded in composite membrane. Recently, Ma et al. (Ma, Burher, Hsiao, & Chu, 2011b; Ma et al., 2012) showed that pore size of CNCs nano-enabled membrane decreased with increased concentration of functional materials.

3.5. Mechanical stability

The mechanical properties of uncross-linked and cross-linked nanocomposites were summarized in Table 3.

The tensile strength of the uncross-linked membrane was 0.98 MPa whereas that of cross-linked ones was 1.1 MPa. The modulus values increased from 128 MPa to 318 MPa after cross-linking. The strain at break showed no difference before and after cross-linking. The low mechanical performance is attributed to the fabrication method used viz. freeze-drying, that restricts the hydrogen bonding between CNCs as well as with the matrix phase and thereby resulting in a loosely bound structure. This processing method used is therefore not the best option in terms of mechanical performance but is good for having well dispersed nanoparticles and a porous structure. Furthermore, the positive impact of cross-linking on mechanical properties was significant especially with respect to modulus of elasticity.

3.6. Flux measurement of composite membranes

The permeability of pure water through the composite nano-structured membrane was 64 L m⁻² h⁻¹ MPa⁻¹. The flux values of tested membrane first decreased slowly during the filtration process because of the scaffold compaction. It was found that the stable permeation flux of composite membrane was reached after 1 h of operation. Ma et al. (2011a) had reported that the flux through a microfiltration membrane using CNCs as infused entity within PAN nanofibrous scaffold was 59 L m⁻² h⁻¹ kPa⁻¹ and much higher than commercial membrane, GS0.22 (25 L m⁻² h⁻¹ kPa⁻¹). The freeze-dried nanocomposite membranes presented in the current work showed lower water permeation flux as compared to both reported membranes, probably due to the high membrane thickness (250–270 μm). However, in the current case low flux is not considered as a disadvantage as increased contact time favors adsorption.

Table 4

Effect of dose of dyes on the removal of dyes.

Doses of dyes (mg/L)	Removal %		
	Methyl Violet 2B	Rhodamine 6G	Victoria Blue 2B
1	91 ± 1.7	70 ± 2.1	98 ± 1.2
5	60 ± 2.3	31 ± 1.9	95 ± 1.3
10	48 ± 1.4	13 ± 1.1	88 ± 1.7

Composite membranes were of 30 × 20 mm in size, standardized values of pH and incubation time were used.

3.7. Dyes removal

The pH conditions, time of incubation and the pollutant concentrations are considered as important parameters that affect the efficiency of dye adsorption. The effect of pH on the percentage of dyes removal from aqueous model wastewater by composite membranes is illustrated in Fig. 3.

Effect of pH was determined by incubation of hybrid composite membranes for 24 h with dyes solutions (1 mg/L) having pHs 5.01, 7.02 and 9.02 at room temperature. In these experiments, the initial solution pH was adjusted to the desired value (pH value 5–9) using either 1 M HCl or 1 M NaOH solutions. Variation in pH can affect the surface charge potential of the adsorbent and degree of ionization. As the surface charge potential decreases with an increase in the solution pH, the electrostatic attraction between positively charged dyes and the surface of adsorbent (composite membrane) is lowered, which may result in an decrease in the rate of adsorption. Fig. 3 shows the maximum percentage removal of dyes from model wastewater at pH 5.01 and the removal percentage decreases with the increase in pH values. The negative zeta-potential of CNC and its dependence on pH was reported in our earlier study (Liu et al., 2014). The functionality of the membranes showed a direct dependence on the zeta-potential of CNC suggesting that surface characteristics of CNC determine the efficiency of adsorption.

The optimum value of pH was chosen as 5.01 and used in the study of the effect of incubation time. The incubation times were varied between 12 and 36 h in dyes solutions (1 mg/L, pH 5.01) at room temperature. The results are shown in Fig. 3. Optimal removal efficiency of composite membranes was observed for 24 h of incubation time for all dyes.

The optimal values of incubation time (24 h) for all dyes and pH were further used for the determination of the dyes doses for the experiments. Table 4 shows the adsorption capacity of fabricated composite membrane at different concentrations. The adsorption

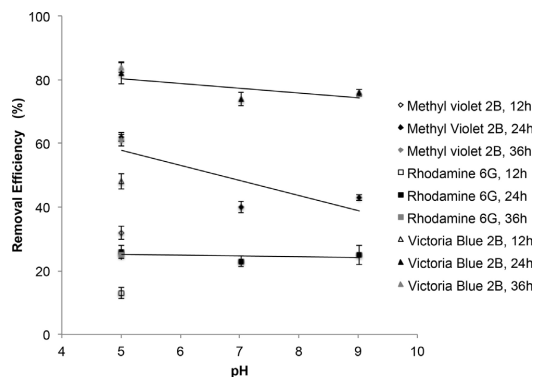


Fig. 3. Graph showing the effect of pH and incubation time on the adsorption of Methyl Violet, Rhodamine 6G and Victoria Blue.

Table 5
Effect of composite membrane on removal of dyes.

Types of dyes	Percentage removal of dyes	
	Uncross-linked membrane	Cross-linked membrane
Methyl Violet 2B	90 ± 2.3	84 ± 1.8
Rhodamine 6G	71 ± 1.6	69 ± 4.2
Victoria Blue 2B	98 ± 3.1	98 ± 3.4

The percentage removal was calculated as mentioned in Eq. (1). The solution treated with 0.2% chitosan membrane was used to measure the value of control.

capacity of composite membrane decreased with increase in the concentration of dyes. Approximately, complete removal (98%) of Victoria Blue 2B was recorded at 1 mg/L concentration. It was inferred that 1 mg/L was the upper limit of dye dosage to evaluate the percentage removal of dyes.

3.8. Removal of dyes with standardized parameters

Targeted dyes having positively charged species were used to determine the adsorption effectiveness of uncross-linked and cross-linked membranes. It was noted that both the membranes were stable in water during the experiments and the cross-linked system showed enhanced dimensional stability which may be attributed to the binding of CNCs in a three dimensional network of chitosan polymer chains. The uncross-linked composites showed slight swelling after contact with dye solutions but were not significant enough to affect the performance.

Table 5 summarizes the dyes removal reached at 24 h by uncross-linked and cross-linked membranes for all dyes solutions. Fig. 4 gives the visual illustration for the removal of dyes by cross-linked composite membranes. It was found that all the dyes showed good adsorption on the membranes being the highest for Victoria Blue followed by Methyl Violet and Rhodamine 6G irrespective of the cross-linking. It is also noted the cross-linking did not have significant impact on the adsorption capability of the membranes. This suggests that the matrix does not influence the adsorption efficiency as it is a minor component (10 wt%) and also due to presence

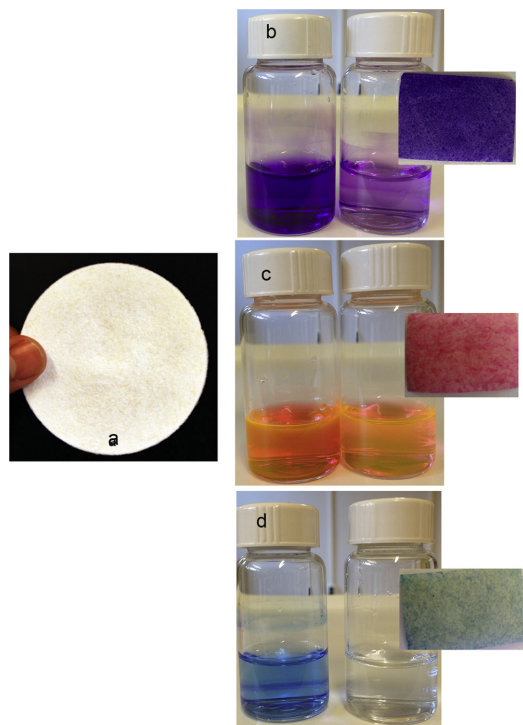


Fig. 4. A schematic representation of experiment shows the naked eyes detection of removal efficiency of cross-linked composite membrane. (a) Photograph of the membrane, water before and after adsorption test for (b) Methyl Violet, (c) Rhodamine 6G and (d) Victoria Blue and the membranes with respective adsorbed dyes.

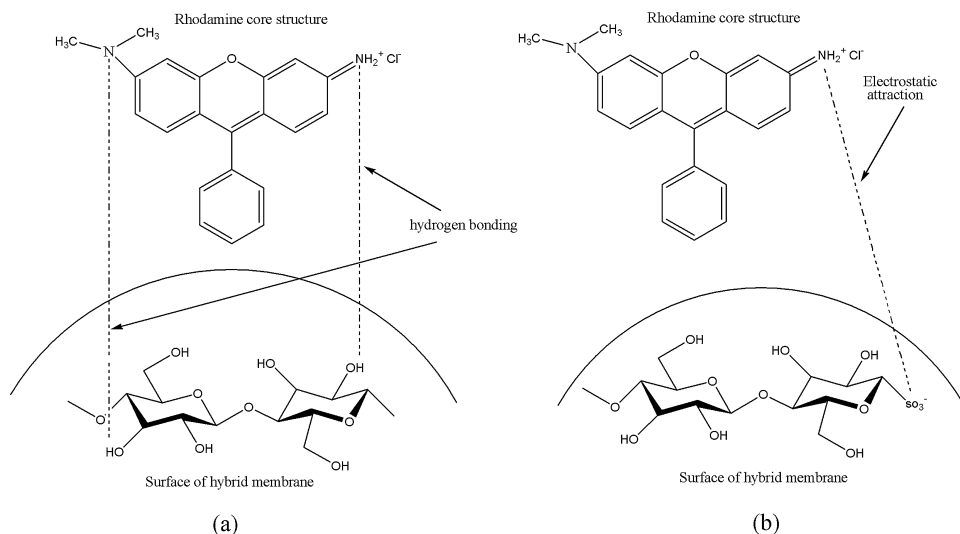


Fig. 5. A schematic representation of the mechanisms of binding of the dyes with CNCs via (a) hydrogen bond formation and (b) electrostatic attraction.

of same charge (positive charge) on surface. This also indicates that the CNCs, which are loosely bound by the matrix are well individualized due to freeze-drying method used and act as the functional entity for capturing the dyes.

The adsorption of dyes may be driven by (i) specific characteristics of dyes (charge, charge potential, functional groups responsible for binding with adsorbent, etc.) and (ii) specific affinity of the dyes for the adsorbent. These kinds of attractions may be predominantly of electrical, van der Waals or chemical nature leading to adsorptions driven by dispersion forces, complexation, hydrogen bond or electrostatic interaction (Al-Ghouthi et al., 2010). CNCs with high negative charges on the surface (as confirmed by zeta-potential values) and targeted dyes having positive charges as shown in Table 1, which leads to electrostatic interaction between the pollutants (dyes) and fabricated composite membranes. Fig. 5 further illustrates the electrostatic attraction between dyes molecules and the cellulose- O^- on the membrane surface. Other researchers also in dye removal reported similar mechanisms from water.

Kaewprapit, Hequet, Abidi, and Gourlot (1998) showed the adsorption of methylene blue dye on cotton fiber (cellulose structure) due to the formation of stable ionic bonds between membrane surface and dyes molecules, which prevent dyes molecules from being eluted from the membrane surface. In another study a micro-nano structured poly(ethersulfones)/poly(ethyleneimine) nanofibrous membrane was fabricated and utilized as an adsorbent for three anionic dyes viz., Sunset Yellow, Fast Green and Amaranth (Min et al., 2012). These researchers had further demonstrated that the species of charge present on the surface of composite determined the maximum adsorption of positively charged dye due to the interaction of positive and negative charges.

4. Conclusion

Isolated CNCs isolated from low cost sludge from industrial cellulose production was used as functional entity for the preparation of fully biobased nanocomposite membranes with chitosan as a matrix. Cross-linking of nanocomposite showed positive impact on mechanical stability and dimensional stability in moist environment and also resulted in slight decrease in surface area and pore size. The pore diameter was found to be in 13–17 nm range and classifies these membranes as ultrafiltration membranes. The higher efficiency for the removal of dyes was observed, being the highest for Victoria Blue (98%), followed by Methyl Violet (90%) and Rhodamine 6G (78%). Two mechanisms were proposed for dyes adsorption onto the membrane, hydrogen bonding and electrostatic interaction. Furthermore, the membranes showed low flux ($64 \text{ L m}^{-2} \text{ h}^{-1} \text{ MPa}$), which supports the usefulness of composite membranes as adsorbents. The high efficiency of the membranes, in terms of adsorption was attributed the freeze-drying process used, which resulted in well individualized CNCs which act as functional entities which were loosely bound together by chitosan polymer chains locked in a 3D network via cross-linking. It may however be noted that freeze-drying adversely affected the mechanical performance of the membranes and will be addressed in the future studies.

Acknowledgements

The authors gratefully acknowledge the financial support by European Commission, under NanoSelect project, EU FP7-NMP4-SL-2012-280519. Iftekhar Uddin Bhuiyan, Luleå University of Technology, is acknowledged for support with BET.

Appendix A. Supplementary data

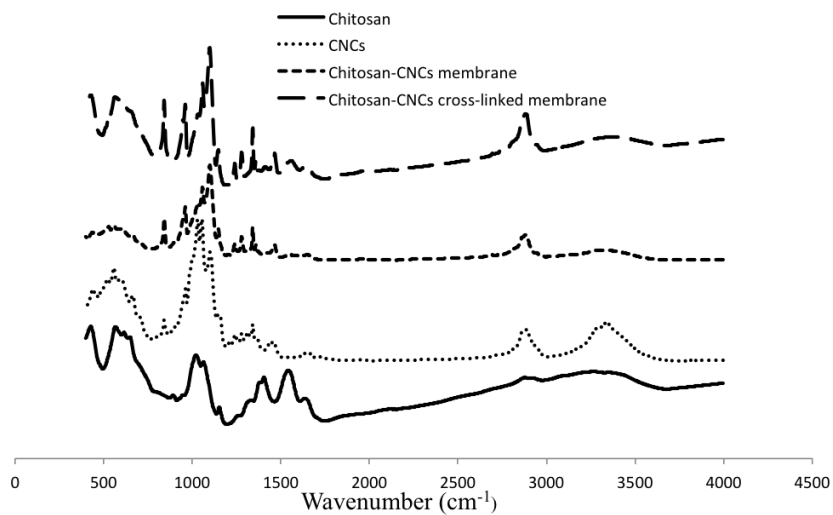
Supplementary material related to this article can be found, in the online version, at <http://dx.doi.org/10.1016/j.carbpol.2014.06.048>.

References

- Al-Ghouthi, M. A., Li, J., Salamh, Y., Al-Laqtah, N., Walker, G., & Ahmad, M. N. M. (2010). Adsorption mechanism of removing heavy metals and dyes from aqueous solution using date pits solid adsorbent. *Journal of Hazardous Materials*, 176, 510–520.
- Araki, J., Wada, M., Kuga, S., & Okani, T. (2000). Birefringent glassy phase of a cellulose microcrystal suspension. *Langmuir*, 16, 2413–2415.
- Bingjie, L., Dongfeng, W., Guangli, Y., & Xianghong, M. (2013). Adsorption of heavy metal ions, dyes and proteins by chitosan composite and derivatives – A review. *Journal of Ocean University of China*, 12, 500–508.
- Bondeson, D., Mathew, A., & Oksman, K. (2006). Optimization of isolation of nanocrystals from microcrystalline cellulose by acid hydrolysis. *Cellulose*, 13, 171–180.
- Brown, E. E., Laborie, M. P., & Zhang, J. (2011). Glutaraldehyde treatment of bacterial cellulose/fibrin composite: Impact on morphology, tensile and viscoelastic properties. *Cellulose*, 4, 1–11.
- Crini, G. (2006). Non-conventional low-cost adsorbents for dye-removal: A review. *Bioresources Technology*, 97, 1061–1085.
- Dhermendra, K. T., Behari, J., & Prasenjit, S. (2008). Application of nanoparticles in wastewater treatment. *World Applied Sciences Journal*, 3, 417–433.
- Diallo, M. S., Christie, S., Swaminathan, P., Johnson, J. H., & Goddard, W. A. (2005). Dendrimer enhanced ultra-filtration recovery of Cu (II) from aqueous solutions using Gx-NH₂-PAMAM dendrimers with ethylene diamine core. *Environmental Science and Technology*, 39, 1366–1377.
- Dural, M. U., Cavas, L., Papageorgiou, S. K., & Katsaros, F. K. (2011). Methylene blue adsorption on activated carbon prepared from *Posidonia oceanica* (L.) dead leaves: Kinetics and equilibrium studies. *Chemical Engineering Journal*, 168, 77–85.
- Gebald, C., Wurzbacher, J. A., Tingaut, P., Zimmermann, T., & Steinfeld, A. (2011). Amines-based nanofibrillated cellulose as adsorbent for CO₂ capture. *Environmental Science and Technology*, 45, 9101–9108.
- Huang, C. H., Chang, K. P., Ou, H. D., Chiang, Y. C., & Wang, C. F. (2011). Adsorption of cationic dyes onto mesoporous silica. *Microporous and Mesoporous Materials*, 141, 102–109.
- Han, J., Zhou, C., Wu, Y., Liu, F., & Wu, Q. (2013). Self-Assembling behavior of cellulose nanoparticles during freeze drying: Effect of suspension concentration, particle size, crystal structure and surface charge. *Biomacromolecules*, 14, 1529–1540.
- Kaewprapit, C., Hequet, N., Abidi, J. P., & Gourlot, J. (1998). Application of methylene blue adsorption to cotton fiber specific surface area measurement. Part I: Methodology. *Journal of Cotton Science*, 3, 164–173.
- Kvien, I., Tanem, B. S., & Oksman, K. (2005). Characterization of cellulose whiskers and its nanocomposite by atomic force and electron microscopy. *Biomacromolecules*, 6, 3160–3165.
- Li, N., & Bai, R. B. (2005). Copper adsorption on chitosan–cellulose hydrogel beads: Behaviors and mechanisms. *Separation and Purification Technology*, 42, 237–247.
- Li, N., Bai, R. B., & Liu, C. (2005). Enhanced and selective adsorption of mercury ions on chitosan beads grafted with polyacrylamide via surface-initiated atom transfer radical polymerization. *Langmuir*, 21, 11780–11787.
- Lin, Y. F., Chen, H. W., Chien, P. S., Chiou, C. S., & Liu, C. C. (2011). Application of bifunctional magnetic adsorbent to adsorb metal cations and anionic dyes in aqueous solution. *Journal of Hazardous Materials*, 185, 1124–1130.
- Liu, P., Sehaqui, H., Tingaut, P., Wichser, A., Oksman, K., & Mathew, A. P. (2014). Biobased nanomaterials for capturing silver ions (Ag⁺) from water via surface adsorption. *Cellulose*, 21, 449–461.
- Liu, C. C., Wang, M. K., & Li, Y. S. (2005). Removal of nickel from aqueous solution using wine processing waste sludge. *Industrial and Engineering Chemistry Research*, 44, 1438–1445.
- Ma, H., Burger, C., Hsiao, B. S., & Chu, B. (2011). Ultra-fine cellulose nanofibers: New nano-scale materials for water purification. *Journal of Materials Chemistry*, 21, 7507–7510.
- Ma, H., Burger, C., Hsiao, B. S., & Chu, B. (2011). Ultrafine polysaccharide nanofibrous membrane for water purification. *Biomacromolecules*, 12, 970–976.
- Ma, H., Burger, C., Hsiao, B. S., & Chu, B. (2012). Nanofibrous microfiltration membrane based on cellulose nanowhiskers. *Biomacromolecules*, 13, 180–186.
- Mathew, A. P., Laborie, M.-P., & Oksman, K. (2009). Cross-linked chitosan/chitin crystal nanocomposites with improved permeation selectivity and pH stability. *Biomacromolecules*, 10, 1627–1632.
- Mathew, A. P., Oksman, K., Pierron, D., & Harmand, M.-F. (2012). Fibrous cellulose nanocomposite scaffolds prepared by partial dissolution for potential use as ligament or tendon substitutes. *Carbohydrate Polymers*, 87, 2291–2298.
- Mikkonen, K. S., Mathew, A. P., Pirkkalainen, K., Serimaa, R., Xu, C., Willfor, S., et al. (2010). Glucmannan composite film with cellulose nanowhiskers. *Cellulose*, 17, 69–81.
- Min, M., Shen, L., Hong, G., Zhu, M., Zhang, Y., & Wang, X. (2012). Micro-nano structure poly(ether sulfones)/poly(ethyleneimine) nanofibrous affinity membrane for adsorption of anionic dyes and heavy metals ions in aqueous solution. *Chemical Engineering Journal*, 197, 88–100.

- Muzzarelli, R. A. A. (2012). Nanochitins and nanochitosans, paving the way to eco-friendly and energy-saving exploitation of marine resources. *Polymer Science: A Comprehensive Reference*, 10, 153–164.
- Muzzarelli, R. A. A., Morganti, P., Morganti, G., Palombo, P., Palombo, M., Biagini, G., et al. (2007). Chitin nanofibrils/chitosan glycolate composites as wound medicaments. *Carbohydrate Polymers*, 70, 274–284.
- Narges, N., Algan, C., Jacobs, V., John, M., Oksman, K., & Mathew, A. P. (2014). Electrospun chitosan-based nanocomposite mats reinforced with chitin nanocrystals for wound dressing. *Carbohydrate Polymers*, 109, 7–15.
- Pavia, D. L., Lampman, G. M., & Kriz, G. S. (2002). *Introduction to spectroscopy. A guide for students of organic chemistry*. Mexico: Thomson Learning.
- Petersson, L., Kvien, I., & Oksman, K. (2007). Structure and thermal properties of poly(lactic acid)/cellulose whiskers nanocomposite materials. *Composites Science and Technology*, 67, 2535–2544.
- Samir, M. A., Alloin, F., & Dufresne, A. (2005). Review of recent research into cellulosic whiskers, their properties and their application in nanocomposites field. *Biomacromolecules*, 6, 612–626.
- Saxena, A., Elder, T. J., Pan, S., & Ragauskas, A. J. (2009). Novel nanocellulosic xylan composite film. *Composites: Part B*, 40, 727–730.
- Shigemasa, Y., Matsuura, H., Sashiwa, H., & Saimoto, H. (1996). Enzymatic degradation of chitins and partially deacetylated chitins. *International Journal of Biological Macromolecules*, 18, 237–242.
- Strand, S., Sauperl, O., & Fras-Zemljic, L. (2010). *Cellulose fibers functionalized by chitosan: Characterization and application*. In M. Elnashar (Ed.), *Biopolymer*. ISBN: 978-953-307-109
- Wesenberg, D., Kyriakides, I., & Agathos, S. N. (2003). White-rot fungi and their enzymes for the treatment of industrial dye effluents. *Biotechnology Advances*, 22, 161–187.
- Xiao, S., Shen, M., Guo, R., Huang, Q., Wang, S., & Shi, X. (2010). Fabrication of multi-walled carbon nanotube-reinforced electrospun polymer nanofibers containing zero-valent iron nanoparticles for environmental applications. *Journal of Materials Chemistry*, 20, 5700–5708.

Supplementary file



FTIR spectra of chitosan, CNCs and composite membranes

Paper C

High flux affinity membranes based on cellulose nanocomposites for removal of heavy metal ions from industrial effluents

Zoheb Karim^{1,2}, Aji P. Mathew¹, Mojca Bozic³, Vanja Kokol³, Jiang Wei⁴, Mattias Grahn²,
Kristiina Oksman¹,

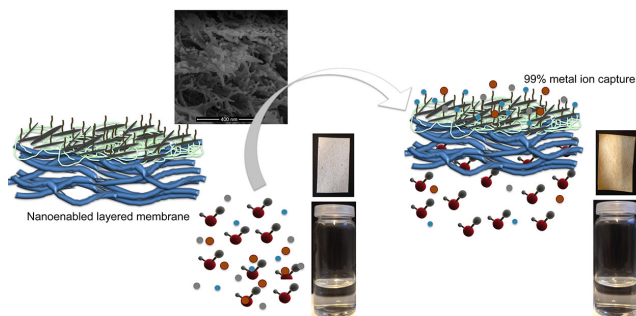
¹Division of Materials Science, Luleå University of Technology
97187, Luleå, Sweden

²Department of Civil, Environmental and Natural Resources Engineering, Division of
Sustainable Process Engineering
97187, Luleå, Sweden

³University of Maribor, Institute for Engineering Materials and Design, Smetanova ulica 17,
SI-2000 Maribor, Slovenia

⁴Alfa Laval Naskov A/S, Business Center Membranes, Stavangervej 10, DK-4900, Naskov,
Denmark

Graphical abstract



ABSTRACT

There is an urgent need to develop point-of-use or point-of-entry water cleaning products that are cheap, environmental friendly and efficient. Fully biobased nanoenabled membranes (NEMs) were processed and successfully used for $\approx 100\%$ removal of heavy metal ions from mirror industry effluents. Layered composite membranes were fabricated using cellulose sludge as support layer and three nanocelluloses (CNC_{SL}, CNC_{BE}, PCNC_{SL}) in gelatin matrix as functional layer. Scanning electron microscopy (SEM) studies revealed the bi-layered morphology of the membrane and well-individualized nanocelluloses in the functional layer. Mirror industry effluent laden with metal ions (Ag⁺ and Cu²⁺/Fe³⁺) when treated with composite membranes, showed high ion removal capacity, being 100% for PCNC_{SL} followed by CNC_{BE} than CNC_{SL}. PCNC_{SL} based membranes successfully reduced the ion concentrations to WHO acceptable limits for Cu²⁺, Fe³⁺ and Ag⁺ ions in fresh water. The removal of metal ions was expected to be driven by the electrostatic attraction between negatively charged nanocellulose and the positively charged metal ions. Bubble point measurements confirmed that the membrane pore structure was in microfiltration range (5.0 - 6.1 μm), which provided very high water permeability (900-4000 $\text{Lh}^{-1}\text{m}^{-2}$) at pressures of < 1.5 bars. The membranes had a tensile strength of 16 MPa in dry conditions and a wet strength of 0.2 MPa, and considered to be potentially used in spiral wound modules.

INTRODUCTION

Over the past two decades, environmental regulations have become more stringent on heavy metal concentrations, which demands improved and innovative water treatment technologies. In recent years, a wide range of treatment technologies such as chemical precipitation, coagulation–flocculation, flotation, ion exchange and conventional membrane filtration, have been developed for heavy metal removal from contaminated wastewater. However, no individual treatment has been found to be universally effective and applicable for heavy metals removal. Furthermore, drawbacks such as high operational costs due to the chemicals used, high-energy consumption, handling costs for sludge disposal and high pressure for filtration are also noticed (1, 2). It is important to note that the selection of the most suitable treatment for metal-contaminated wastewater depends on the initial metal concentration, the overall treatment performance compared to other technologies, plant flexibility/reliability and environmental impact. All the factors mentioned above should be taken into consideration in selecting the most effective and inexpensive treatment in order to protect the environment (2).

Recently, nanostructured affinity membranes were developed to permit the purification of contaminants based on physical/chemical properties or biological functions. Rather than operate purely on the sieving mechanism, affinity membrane based on its separation on the selectivity of the membrane to ‘capture’ contaminants, by immobilizing specific ligands or produce specific functional groups onto the surface of membranes. Affinity membrane reflects technological advances in both fixed-bed liquid separation and membrane filtration, and combines both the outstanding selectivity and the reduced pressure drops associated with filtration membranes (3).

Few works have been reported on the application of nanocellulose for the removal of heavy metals. A novel micro-nano structure poly(ether sulfones)/poly(ethyleneimine) nanofibrous membrane was fabricated with nanocrystals and functional additives and utilized as an adsorbent for anionic dyes and heavy metal ions from aqueous solution by Chu and coworkers from Stony Brook University (4, 5). However these studies mostly used it on a non-biobased substrate or support layer. We aim to develop fully biobased nanocellulose membranes for water cleaning. A large surface area to volume ratio is one of the most important requirements for an ideal affinity membrane (6). Karim et al. (7) have recently

showed that nanocrystals based membranes prepared by freeze drying resulted in low water flux and low mechanical performance, in spite of good functionality (7). Low mechanical properties was attributed to the processing method used, viz. freeze- drying, which reduces H-bonding between nanocrystals and low flux was to the high thickness (250 μ m) of membrane.

In the present study, an improved fully bio-based high flux membrane-(membranes/adsorbents) was fabricated using very simple and fast process, viz. vacuum filtration followed by hot pressing, following the well documented 'nanopaper' process (8, 9). Native and modified cellulose nanocrystals was used as functional entity on a support layer of micro-sized cellulose sludge fibers to fabricate a fully bio-based membrane. It was expected that the networking potential of microscale fibers can be combined with adsorption potential of nanocellulose to tailor efficient water cleaning membranes. The support layer of cellulose sludge micro fibers cuts down the cost of membranes/adsorbents, but provides mechanical and dimensional stability due to H-bonding. Impregnation of functional layer on the support layer was performed via filtration of three nanocellulose materials embedded in gelatin matrix on to the support. The morphology of the membranes and dispersion on nanoparticles in the functional layer was studied SEM images. Mechanical testing was performed in dry as well as in wet conditions using tensile testing machine. Flux was measured by cross-flow filtration device equipped with temperature and pressure control. Two real wastewater samples containing Ag^+ and $\text{Cu}^{2+}/\text{Fe}^{3+}$ from mirror industry were collected from southern part of Europe (Spain) and have been targeted by fabricated membranes/adsorbents. An adsorption mechanism was also demonstrated to understand the bonding between functional nanocellulose and heavy metal ions. Finally, sorption capacity of applied nanocelluloses has been compared with adsorbents studied before or available in market.

EXPERIMENTAL SECTION

Materials

Non-dried dissolving cellulose residue (sludge) from dissolving cellulose was obtained from Domsjö Fabriker AB, Ornskoldsvik mill, Sweden. Sludge was used as received without any pretreatments. Based on the data from the material supplier, the chemical composition of the

used sludge was, cellulose content (95%), hemicellulose (4.75%) and very low content of lignin.

Gelatin and polyethylene glycol (PEG 2000) were purchase from Sigma-Aldrich (USA). Acetic acid and sulfuric acid were supplied by VWR (BDH, France).

Isolation and surface modification of nanocellulose

The process routes used to prepare cellulose nanocrystals used in the study as functional entity are schematically shown in Fig. 1. Cellulose nanocrystals (CNC_{SL}) were isolated from cellulose sludge using sulphuric acid hydrolysis as reported by Karim et al (7).

Unbarked wood was hydrolyzed using dilute acid in a bioethanol pilot plant and refined by solvent extraction and bleaching to obtain pure cellulose. Cellulose, after bioethanol process in a plant was supplied by SP Processum, Örnköldsvik, Sweden (17 wt%). The purified cellulose from bioethanol process was made into 2 wt% suspensions, mixed by shear mixture and passed through the homogenizer, 10 times to obtain a thick gel of cellulose nanocrystals (CNC_{BE}) as reported earlier by Mathew et al (10).

The CNC_{SL} were enzymatically modified to introduce phosphoryl groups on the surface. Reaction was carried out accordingly to Bozic et al. (11). Briefly, reaction proceed in 0.9 wt% of CNC_{SL} phosphate buffer (pH 7.6) dispersion in the presence of a 50 mM ATP, 250 mM of MgCl₂ and 35 U/ml of hexokinase enzyme for 24 h at 30°C. After the protein deactivation, PCNC_{SL} were washed several times (centrifuged at 6000 rpm for 4 min) with distilled water, until no ATP absorption peak at 260 nm could be detected.

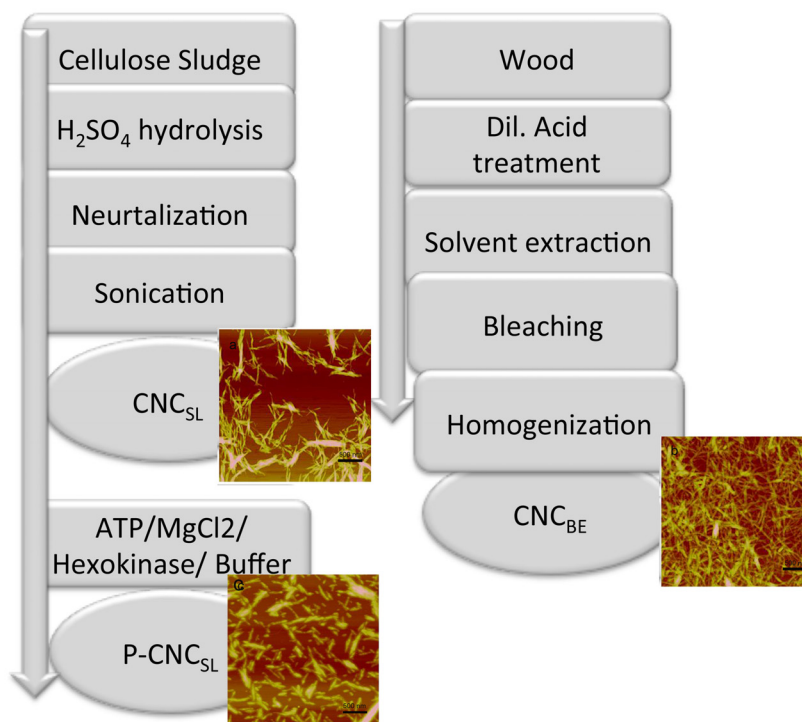


Fig. 1: Isolation processes of functional entities.

Processing and characterization of membranes/adsorbents

A very simple and fast method, vacuum-filtration was used to formulate thin-layered nanocomposite membranes. The 2 wt % of sludge was used to form layer of support. The fabrication of thin functional layer was performed by further filtration of nanocellulose (CNC_{BE}, CNC_{SL} and PCNC_{SL}) gelatin hybrid suspension as shown in Fig 2. Concentrated nanocellulose suspensions and gelatin (1 wt% each) were taken in 1:1 to form functional layer. After 12 h drying in room temperature, the prepared porous composites were pressed between aluminum plates in a compression-molding machine with load of 60-70 kN. (Fontune Presses, Elastocon, Sweden) with heating to obtain compacted membranes

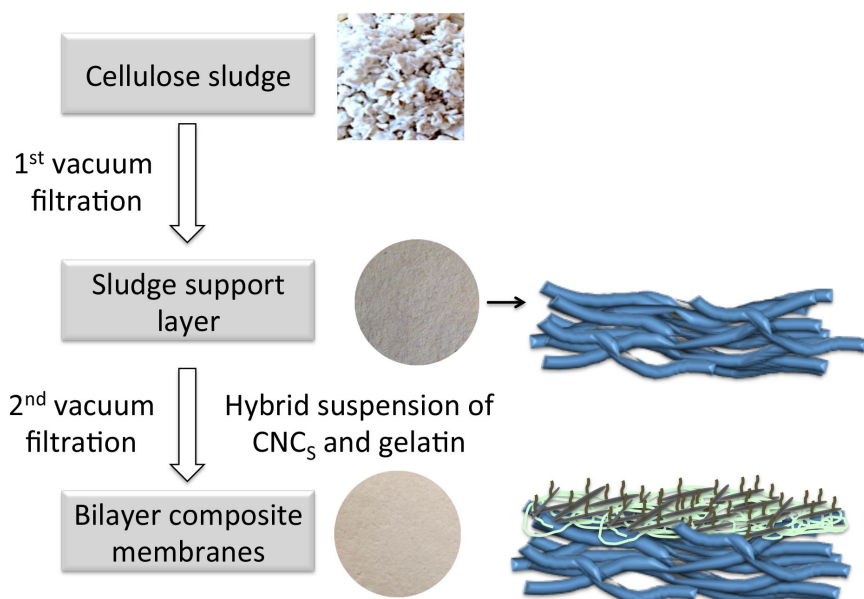


Fig. 2: Fabrication process of composite membranes

Characterization methods

Microscopy

An atomic force microscope (Nanoscope V, Veeco Instruments, Santa Barbara, CA, USA) was used to examine the morphologies of the CNC_{SL} , CNC_{BE} and PCNC_{SL} . A drop of diluted suspension of each nanoparticle was deposited onto freshly cleaved mica and left to dry at room temperature and was scanned in tapping mode. The cantilever resonance frequency was 350 kHz and the spring constant was $10 - 200 \text{ nm}^{-1}$. The diameter measurements were conducted with the aid of Nanoscope V software.

The morphology of thin-layered composite membranes was examined at high magnification power using MAGELLAN 400, SEM (FEI Company). The membranes were fractured in liquid nitrogen and sputter coated with tungsten. The nanocomposite membranes were observed in the SEM at an acceleration voltage of 3 kV.

The PCNC_{SL} membranes was prepared with ion-milling to obtain a clean cross-section and coated with tungsten and observed in the SEM at an acceleration voltage of 3 kV.

Mechanical properties

The tensile tests of the thin-layered composite membranes in dry as well as in wet condition were performed using a Universal Testing Machine, Shimadzu Autograph AG-X (Japan), with a load cell 1KN and the gauge length was 20 mm. Test specimens were 5.0 mm and in the range of 0.500-0.550 mm in nominal width and thickness, respectively as measured by digital caliper. The samples were stretched with 2 mm/min crosshead speed until failure. Stress at break (MPa), max strain (%) and modulus of elasticity were calculated as described elsewhere (7).

Determination of surface area using BET

N₂ adsorption using Brunauer-Emmett-Teller (BET) method with sample degassed instrument (Micromeritics ASAP 2020) automated system was used for the determination of surface area. The nanostructured composite membranes first degassed in the Micromeritics ASAP 2020 at 115 °C for 4 h prior to the analysis by N₂ adsorption at -196 °C. BET analysis was carried out for a relative vapor pressure of 0.01-0.3 at -196 °C.

Evaluation of heavy metals adsorption on biobased composite

Two real wastewater samples (from mirror making industry) contaminated with Ag⁺ and Cu²⁺/Fe³⁺ were obtained from southern part of Europe. All samples (10 ml each) were incubated with thin-layered nanocomposite membranes (30 x 20 mm) with stirring for 24 h to complete the adsorption process. The stirring of polluted water is done to ensure constant contact of metal ions to the surface of composite membranes and to increase the adsorption efficiency. A control experiment was also performed with sludge/gelatin composite membrane. The remaining polluted water after incubation was measured by inductively coupled plasma-optical emission spectrometer (ICP-OES). The ICP-OES with a radial torch was used to measure the ions concentration in the polluted water of each single sample after metal ions adsorption. The adsorption capacity of membranes for ions was calculated as

mentioned in our previous published article (12).

Metals ions, adsorbed on composite membranes were further characterized using a scanning electron microscope (SEM, JSM-6460 LV, JEOL, USA), equipped with energy dispersive X-ray elemental spectrometry (EDS), having software, Inca Energy, Oxford. Metal ions adsorbed samples were mounted on carbon stubs using double stick tape. Fig.3 shows the experimental flow chart of metal ions adsorption analysis. The adsorbed membranes were scanned with the depth of around 2 μm to detect the presence of metal ions. The electron beam of 20 kV was applied to determine the presence of ions. The elementary weight ratio and atomic ratio were determined and reported.

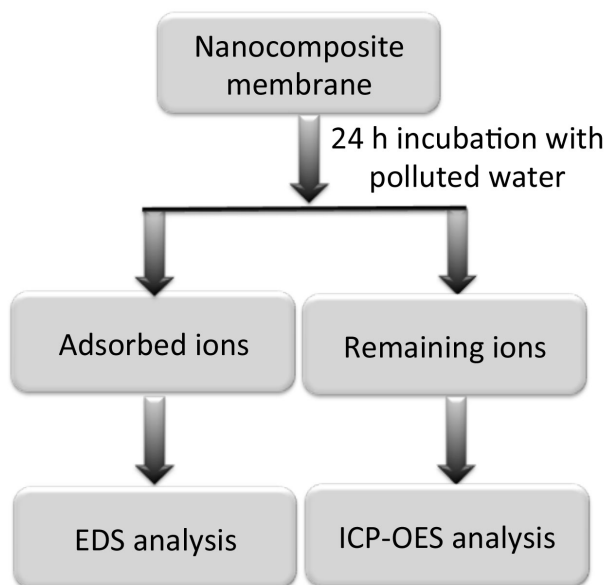


Fig. 3: Schematic representation of metal ions removal experiment

Pore size determination

The average pore size was measured for membranes based on CNC_{BE} and PCNC_{SL} by bubble point method using PMI Capillary Flow Porometer from porous Materials, Inc. USA, to test our membranes at industrial level. A membrane is placed in a holder, with specific liquid placed on the topside of the membrane. The use of water as a test solution for all types of membrane isn't always the best. Water has a surface tension of 72 dynes/cm, and will require a high degree of gas pressure. To solve this, a test solution with a low surface

tension was used.

Measurement of water permeability:

Sludge support and CNC_{BE} and PCNC_{SL} based membranes were used for the measurement of water permeability. A schematic diagram of the experimental apparatus for a cross-flow filtration test is presented in Fig 4. The system consists of a feed tank with a total working volume of 10 L and a filtration module. Thin-layered composite membranes were stored in a 10 L feed tank and then entered a recirculation loop, where a diaphragm pump sustained the recirculation flow rate. A backpressure valve was located in the recirculation loop to adjust the trans-membrane pressure. Permeate which was collected in a reservoir on an electronic balance to measure the flux was returned into the feed tank for total recycling. The water in the recirculation loop was maintained at 25 °C by thermostat. The total surface area of membrane used was approximately 0.0169 m², which was sufficiently compared with the working volume of feed water. The water permeability of membranes was determined up to burst pressure (1.5 bar) starting from 0.5 bars.

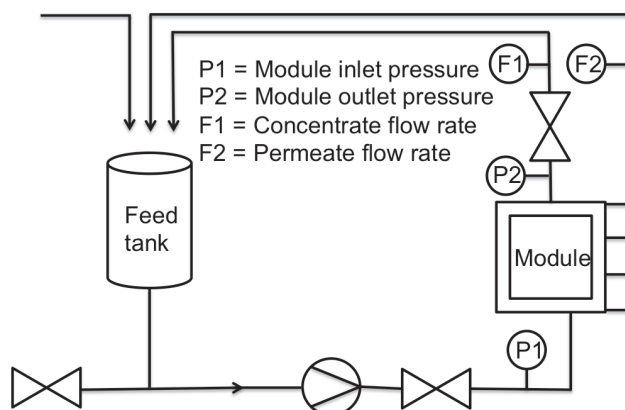


Fig. 4: Cross-flow filtration system scheme

RESULTS AND DISCUSSION

Morphology of the cellulose nanocrystals

Figure 1 shows the AFM images of the used cellulose nanocrystals in the membrane fabrication. CNC_{SL} and CNC_{BE} shows typical cellulose nanocrystal structure and the diameters were found to be in the range of 5-10 nms. AFM image of $PCNC_{SL}$ have whisker like structures but were shorter and broader than the corresponding non-modified ones. The diameters were found to be in the range of 20 nms, indicating the presence of laterally aggregated CNCs after drying on mica surfaces. The diameters reported are based on the height to compensate the tip broadening effect and were measured using Nanoscope V software. The accurate determination of the length was not possible from the AFM using this method and therefore not presented here. However, the AFM image shows that CNC_{BE} are longer compared to CNC_{SL} and $PCNC_{SL}$.

Morphology of nanocomposite membranes

The thickness of the support later was 430 μm and increased to 440-448 respectively, after the impregnation with the functional layer. The thickness of functional layer of CNC_{SL} , CNC_{BE} , and $PCNC_{SL}$ determined based on the thickness difference were 10, 18 and 11 μm , respectively. The thickness difference for the functional layers may be assigned to the dimensions of nanocrystals and the relative degree of impregnation of gelatin/CNCs suspension into the support layer.

The morphology of the support and the layered nanocomposite membranes at the micro/nanometer length scale were observed using SEM and are shown in Figure 5. In Figure 5a the surface and the cross-section of the support layer are given where micro-sized fibers were clearly visible and the fibers are loosely bound together in a 3D network, with microscaled voids in between.

The bi-layered membrane cross-sections for S-G/ CNC_{SL} , S-G/ CNC_{BE} , S-G/ $PCNC_{SL}$ are shown in Fig. 5 b-d. Bi-layered morphology of fabricated nanocomposite membranes was in agreement with previous reports by de-Mesquita et al. (13). In all SEM images in the left

column a surface functional layer is clearly visible on the support layer. However, the depth of impregnation varied from sample to sample and it was not possible to see any nanocrystals impregnated into the support layer at this magnification. SEM images in the middle column shows that the functional layer on the top was found to be made up of layered structures in all cases.

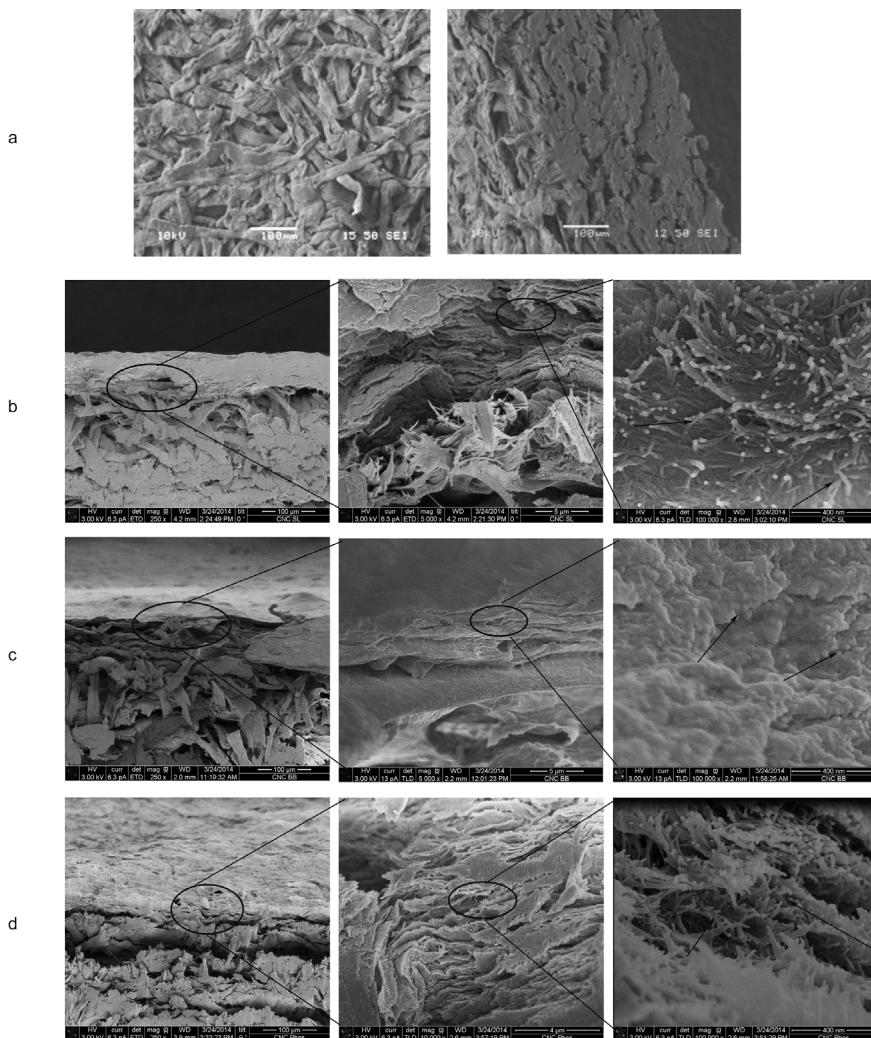


Fig. 5: SEM images of a) support layer (surface and cross-sections) b) S/G-CNC_{SL} c) S/G-CNC_{BE} d) S/G-PCNC_{SL} at different magnifications

The images on the right column shows the functional layer at high magnifications. The high-resolution SEM image of functional layer showed individualised nanoscaled dispersed within the gelatin forming a network of functional entity without visible agglomerates. The good dispersion of nanocelluloses in gelatin matrix indicates positive interaction between gelatin matrix and functional entity. It may be considered that nanocellulose are bound together in a three dimensional network by gelatin chains. Further more, the functional layer also seems to be denser and the nanocrystals more embedded in the matrix in the case of CNC_{BE} compared to CNC_{SL} and PCNC_{SL}.

S/G-PCNC_{SL} membrane cross-section was studied in detail after ion milling to understand the infusion of CNC_{SL} the bi-layered structure and are shown in Fig. 6.

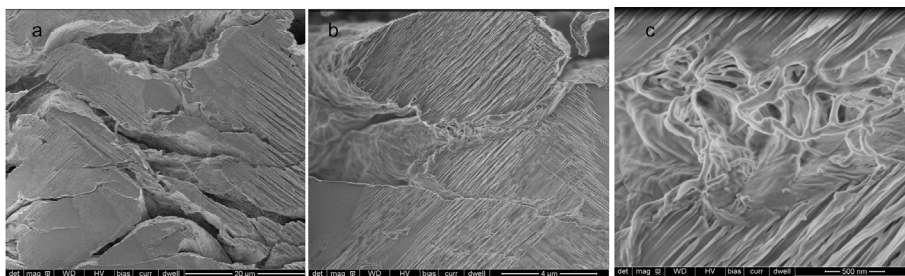


Fig. 6: SEM images of S-G/PCNC_{SL} bilayered membranes showing the infusion of functional layer into the support layer

It was possible to see well-defined support layer and the functional layer in the membranes. The thickness of the functional layer was measured to be 8.5 μm (not shown) and is in agreement with the values calculated based on thickness differences. The fibers near the interphase between support and functional layers were coated with nanocrystals indicating some infusion of functional layer into the support layer. A similar trend is expected for CNC_{SL} based membranes also. However a lower degree of infusion was expected for CNC_{BE} compared to CNC_{SL} and P-CNC_{SL}, due to the presence of longer nanocrystals and probably explain the higher thickness of the functional layer based on CNC_{BE}. The micro-scaled porosity of the support layer and low thickness of the functional layer confirmed by SEM was expected to provide high flux during water purification while providing sufficient mechanical strength.

Mechanical properties

Mechanical properties of thin-layered composite membranes measured in tensile mode are summarized in Table 1.

Table 1: Mechanical stability of composite membranes

Conditions	Types of membranes	Modulus of elasticity (MPa)	Stress at break (MPa)	Max Strain (%)
Dry	Support	245±0.1	9±0.2	1.2±0.4
	S-G/CNC _{SL}	362±0.3	13±0.3	2.1±0.3
	S-G/CNC _{BE}	647±0.4	19±0.8	2.3±0.1
	S-G/PCNC _{SL}	402±0.9	16±0.5	2.4±0.2
Wet	Support	37±0.4	0.13±0.4	0.9±0.4
	S-G/CNC _{SL}	70±0.2	0.21±0.4	0.49±0.3
	S-G/CNC _{BE}	130±0.7	0.24±0.5	0.30±0.5
	S-G/PCNC _{SL}	92±0.6	0.22±0.6	1.1±0.4

The support alone showed a strength of 9 MPa which increased with the addition of the cellulose nanocomposite functional layer, Higher strength of membranes was observed in the current study (13-19 MPa) compared to our earlier studies on freeze-dried CNC based nanocomposites (2 MPa) (7) and support in this study. It was inferred that the filtration followed by hot pressing used for the preparation of membranes facilitate the formation of hydrogen bonds and thereby provide mechanical stability to the membranes. The tensile strength and the modulus of CNC_{BE} based bi-layered membrane were higher compared to CNC_{SL} and PCNC_{SL} membranes. The strain at break was in the range of 2 % and the differences between membranes were not statistically significant. Recently, an ultrafiltration membrane was reported with CNC infused on nonwoven support of electrospun PAN fibers. Mechanical properties were measured and compared with commercial available GS0.22 ultrafiltration membrane (6); the stress at break of reported composite membrane was 14±0.8 MPa and modulus was 375 MPa. Thus, bi-layered fabricated composite membranes produced in the current study by filtration have comparable tensile strength and higher modulus. It is

worth mentioning that in the current study the support layer is based on cheap bioresidue and the prepared membrane is fully biobased.

The mechanical stability in wet condition follows the same pattern as shown in dry condition but with lower values. The higher mechanical properties on CNC_{BE} based membranes may be due to the denser functional layer compared to CNC_{SL} and P-CNC_{SL} found in SEM studies. The reported tensile strength (even in wet condition) of all fabricated membranes was enough to use them in water cleaning application especially in spiral wound modules (14).

Removal of heavy metal ions

The real polluted water was incubated for 24 h with fabricated membranes to reach maximum removal efficiency and the results are summarized in Table 2. The metal ions removal efficiency of all three nanocomposite functional membranes, is consequently, in the sequence of PCNC_{SL} > CNC_{BE} > CNC_{SL}. The removal rate of PCNC_{SL} functional membrane was 100% for all three metal ions (Cu²⁺, Fe³⁺ and Ag⁺). The percentage removal of ions was lower in the case of CNC_{BE} and CNC_{SL} functional membranes. CNC_{BE} composite membrane has intermediate removal capability, both for Cu²⁺ (33%) and Fe³⁺ (30%) compared to CNC_{SL} functional nanocomposite membrane (only 12 % for Cu²⁺ and Fe³⁺). Thus, the removal rate for CNC_{BE} is two times higher with respect to CNC_{SL}.

Table 2: ICE-OPS analysis of metal ions removal

Types of membranes	pH	C _o (mg/L)	C _i (mg/L)	Sorption capacity		Removal rate (%)	WHO (2004) limit (mg/L)
				Membran e (mg/g)	CNCs (mg/g)		
Cu ²⁺							≤0.005->30
S-G/CNC _{SL}	2.3	330.2	290.2	8	11	12%	
S-G/CNC _{BE}			220.5	22	64	33%	
S-G/PCNC _{SL}			3.0	66	233	99%	
			Fe ³⁺				0.5-50
S-G/CNC _{SL}	2.3	550.5	480.0	14	20	12%	
S-G/CNC _{BE}			380.0	34	100	30%	
S-G/PCNC _{SL}			1.5	109	391	99%	
Ag ⁺							0.005-0.1
S-G/CNC _{SL}	9.1	1.48	0.00	0.29	0.42	100%	
S-G/CNC _{BE}			0.00	0.29	0.87	100%	
S-G/PCNC _{SL}			0.00	0.29	1.0	100%	

The quantity of functional group contents on the surface of fabricated membranes is the reason for the different percentage removal. The sulphate groups present on the surface of CNC_{SL} are 30-90 mmol/kg is lowest compare to carboxylic group on CBC_{BE} (150 mmol/kg) and the highest vale of carboxylic and phosphate groups (425 mmol/kg) are recorded on phosphorylated CNC; therefore, phosphorylated CNC have highest removal percentage of metal ions compare to other used nanocelluloses (11, 15).

Table 3 compares metal ion removal performance of the biobased functional entity used in the current study with adsorbent materials found in literature. Cu²⁺ adsorption from water based on literature reports shows that the best removal rate for chitosan with an efficiency of 70mg/g (16) on chitosan followed by carbon nanotube (67.8mg/g). Bio-based nanomaterials have also been used for the remediation of Cu²⁺; recently two reports confirmed the use of chitin nanofibers and cellulose nanocrystals. The maximum sorption capacity of CNCs was 2.5 mg/g (17) and chitin nanofibers was 141.08 mg/g (18). Our finding confirms the outstanding sorption capacity on used nanocellulose. The PCNC_{SL} has the highest (233 mg/g) followed by CNC_{BE} (64 mg/g).

The sorption capacity of Fe^{3+} is very high for PCNC_{SL} (391 mg/g). One very interesting literature report shows the use of cow bone charcoal for the removal of iron metal ions from industrial wastewater (19) but the sorption capacity of used adsorbent was very low (31.4 mg/g) compared to PCNC_{SL} (391 mg/g) and CNC_{BE} (100 mg/g). Table 3 further describes the WHO (20) prescribed limit for the selected metal ions in fresh water, the concentration of Ag^+ is below the prescribed limit without the saturation. S-G/ PCNC_{SL} composite membranes are able to remove Cu^{2+} and Fe^{3+} within the prescribed range, thus, PCNC_{SL} is more effective compared to CNC_{SL} and CNC_{BE} .

Table 3: Comparison of sorption capacity of used nanocellulose with other adsorbents

Equilibrium sorption capacity of used nanocelluloses (Depends on initial concentration of metal ions)				Maximum sorption capacity of reference adsorbents (from adsorption isotherm modeling)						Ref.
Ion (mg/g)	CNC_{SL}	CNC_{BE}	P- CNC_{SL} *	Alfalfa biomass	Cow bone charcoal	Chitosan	CNCs	Chitin fibers	CNT	
Ag^+ *	0.42	0.87	1.0	27.37	--	--	34.4	--		18, 21
Cu^{2+}	11	64	233	--	--	70	2.5	141.08	67.8	17, 19, 24
Fe^{3+}	20	100	391	--	31	14	--	--		17, 20

*Sorption capacity of Ag^+ and PCNC_{SL} was not at equilibrium. The values reported in the literature are the saturation limit (determined after 10 to 15 cycle of reuse) but in our study only one cycle of adsorption evaluation was performed. Thus, the reusability must be performed in future to find the saturation limit.

The Ag^+ sorption capacity onto the with respect to unit mass of our bilayered membrane or functional entity was lower compared to adsorption results reported by Herrera et al. (21) on the alfalfa biomass (27.37 mg/g) and other available resins; Duolite GT-73 (155.92 mg/g), Diaion WT01S (45.0 mg/g), Diaion CRB02 (15.83 mg/g) and Dowex 66 (48.44 mg/g) (3, 21). The main reason is the initial concentration of Ag^+ . The adsorption capacity reported in

the literature is on saturation limit but on the other hand our findings are limited onto the low initial concentration of Ag^+ (1.48mg/L) but complete removal percentage was recorded. It is also considered that these biobased membranes after adsorption of Ag^+ ions can be converted to an antibacterial device for the treatment of drinking water as reported by Theresa et al. (22). The reuse of Ag^+ ions adsorbed membranes as antibacterial device will be reported in future.

The results show that the PCNC_{SL} based membranes is outstanding among all adsorbents. CNC_{BE} also have quite good sorption capacities for copper and iron ions and the efficiency is the least for CNC_{SL} based membranes.

Mechanism of metal ion removal from water

The bilayered membranes samples, before and after incubating with effluent water were used for elemental constitution analysis and the spectrum is shown in Fig. 7. Only Si, S, C and O can be observed in untreated ones which have been known as the principle elements of fabricated composite membranes. No signals of Ag^+ , Cu^{2+} and Fe^{3+} elements were found in this spectrum. The EDS spectrums of membranes treated with contaminated water show the introduction of new peaks, which confirms the presence of the respective metal ions on the membrane surface. The Ag^+ , Cu^{2+} and Fe^{3+} signals can be observed on the spectrum obtained after treatment with polluted water, indicating that the interaction/immobilization of metal pollutants had occurred on the surface of fabricated functional nanocellulose. The intensity of ions adsorption is higher in the case of PCNC_{SL} than CNC_{BE} followed by CNC_{SL} . Therefore, the efficiency of adsorption is same as found previously in the ICE-OPS results. Thus, ED's analysis provides the direct evidence for the specific adsorption of respective metal ions on the surface of nanocomposite membranes. Our results are in the agreements of previous published data where an attempt has been made to adsorb Cu^{2+} on the surface of iron-coated sand (23). The results are also in agreement with our earlier studies where model and industrial waste water contaminated with heavy metals ions has treated with four nanocellulose functional entities (CNC_{SL} , CNC_{BE} , phosphorylated CNC and phosphorylated CNF (15).

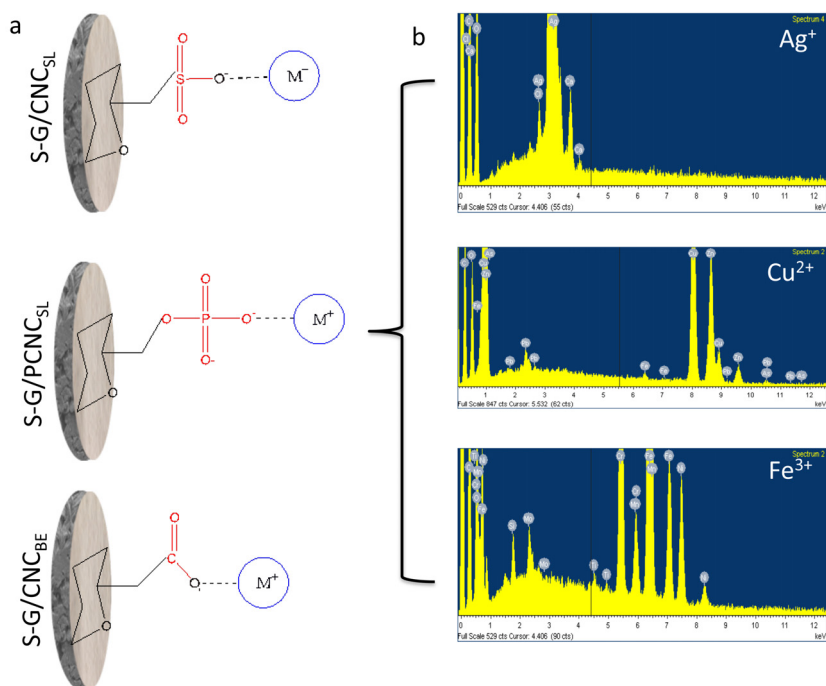


Fig. 7: Approved mechanism for the metal ions adsorption (a) and a confirmation with EDS (b). The EDS results are shown only for S-G/PCNC_{SL} composite membranes and the same pattern have been observed with other two membranes. The scanning area of samples analyzed by EDS was 200 μm^2 and samples were not smooth due to adsorption of heavy metals on the surface of composite membranes. Thus, the results reported here are qualitative.

The reason why these membranes can adsorb metal ions is explained based on the functional groups on the surface. The surface functional groups on the nanocrystals used as functional entity are different and is based on the processing route used. The isolation of CNC_{SL} was performed by sulphuric acid hydrolysis (7) and presence of sulfonate groups (SO₃⁻) was confirmed by FTIR in our previous study (10). The main functional group available on CNC_{BE} after isolation process was carboxylate (-C=OO⁻) and is confirmed by XPS analysis (10). PCNC_{SL} was highly effective for metals ions removal and is due to the introduction of phosphate (PO₃²⁻) group on the surface of CNC_{SL} during hexokinase-mediated reaction, as described previously (11,15). Thus, functional groups appear after the different isolation/functionalization processes are responsible for the adsorption of heavy metals ions. The existences of functional entities are phosphate, carboxylic and sulphonate, on macromolecules chain of PCNC_{SL}, CNC_{BE} and CNC_{SL}, respectively are the main driving force for negative charges on nanocellulose. The possible mechanism for the adsorption of

metal ions on the surface of fabricated nanocomposite is the negative-positive interactions as shown in Fig. 7a.

Pore structure and surface area of the membranes

Bubble point method is very accurate and effective for pore measurement at industrial level. The average pore size of S-G/CNC_{BE} and S-G/PCNC_{SL} membranes was 5.1 and 6.2 μm and confirmed the microfiltration range of composite membranes. The large average pore sizes of composite membranes are beneficial to ensure high flux through the membranes while simultaneously larger surface area related to enhancement of the adsorption efficiency of fabricated composite membranes.

The surface area as obtained from BJH analysis of N_2 gas adsorption isotherm of S-G/CNC_{BE} thin-layered composite membrane was highest (32.6 m^2/g) compared to S-G/CNC_{SL} membrane (26.3 m^2/g) followed by S-G/PCNC_{SL} (18.8 m^2/g) membranes. The lower surface area of all the fabricated membranes is expected as compacting of networks occurs during hot pressing. While comparing the three membranes the main cause for the difference in the surface area may be the depth of infusion of nanocellulose within the support layer and is probably related to the dimensions of cellulose nanocrystals. The CNC_{BE}, which has infused the least provided membranes with highest porosity and highest surface area.

Water filtration performance of nanocellulose composite membranes

The filtration performance of the nanocellulose based membrane, which showed best adsorption performance was evaluated in cross-flow system. Water flux experiments were conducted under the variable rate condition (applied pressure) and Fig. 8 shows the water permeability data as a function of applied pressure during cross-flow. Support has the highest water permeability at all applied pressure owing to the free water flow through microstructure and decreases when the functional layer is present. The water permeability of S-G/CNC_{BE} is low at all applied pressures compared to S-G/PCNC_{SL} and is due to the thicker and denser functional layer in the case of CNC_{BE} membranes. Thicker porous material promotes water movement in a zigzag motion while linear motion has been observed within thinner materials (21,14). The low water flux of CNC_{BE} based composite membranes was further supported by

the average pore size results. Smaller average pore size of support-CNC_{BE} is the third main factor for the low water flux. Ma et al. (6) had reported the flux through a microfiltration membrane using CNCs as infused entity within PAN nanofibrous scaffold was 0.59 Lm⁻²h⁻¹ bar⁻¹ and much higher than commercial membrane, GS0.22 (0.25 Lm⁻²h⁻¹bar⁻¹). Fabricated thin-layered composite membranes in the current study have significantly high flux compared to previous reported membranes as well as the commercially available membranes.

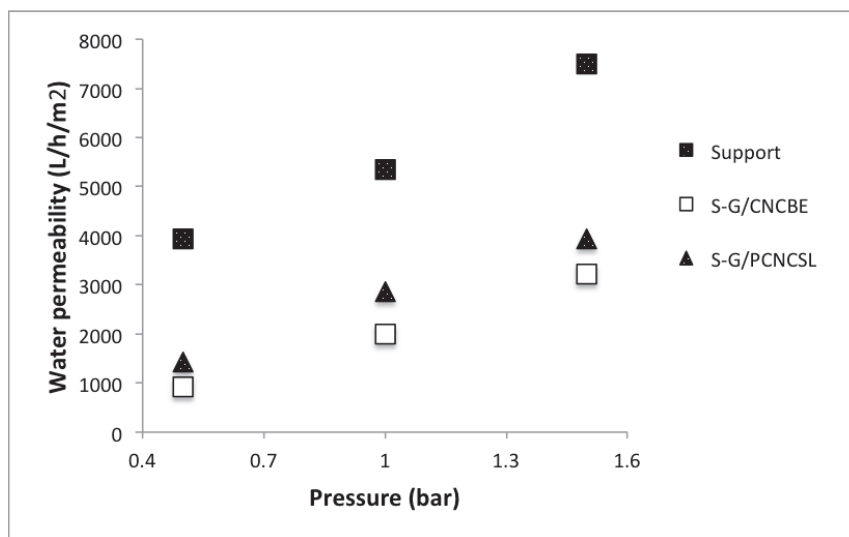


Fig. 8: Water permeability of assigned composite membranes with different pressure

The study demonstrates the successful processing and performance of fully biobased membranes, which has high potential as commercial scale product for metal ions capture from industry effluents. High flux nano-enabled membranes have been achieved following a very simple, fast and effective process, viz. vacuum filtration followed by hot pressing. The morphology of fabricated membranes confirms the bi-layered structure with some degree of infusion of the functional layer into to the support layer. The support layer provided mechanical stability to the material while the functional layer immobilized metal ions from contaminated water. PCNC_{SL} based membranes were most effective for the removal of all three metal ions ($\approx 100\%$ removal) and lowering it to WHO limits for Ag⁺, Cu²⁺ and Fe³⁺ in fresh water. Mechanical strength of all the membranes in wet condition was higher (0.2MPa) than the requirements for use in spiral wound module (0.039 MPa). Water permeability of bi-layered composite membranes was very high due to microporous structure and the adsorption

efficiency after single cycle of adsorption was higher than reference adsorbents found in literature.

Acknowledgments:

The authors gratefully acknowledge the financial support by European Commission, under NanoSelect project, EU FP7-NMPA-SL-2012-280519. Iftekhar Uddine Bhuiyan, Luleå University of Technology, is acknowledged for SEM results.

References:

1. Rattan, R. K.; Datta, S. P.; Chhonkar, P. K.; Suribabu, K.; Singh, A. K., Long-term impact of irrigation with sewage effluents on heavy metal content in soils, crops and groundwater-a case study. *Agri. Ecosys. Environ.* **2005**, *109*, 310–322.
2. Mattuschka, B. R.; Junghans, G.; Stmbe A., Bio-sorption of metals by waste biomass, biohydrometallurgical technology. Proceeding of International Biohydrometallurgy Symposium. Jackson Hole, Wyoming, USA, **1993**, August 22-25.
3. Tomas, J.; Kula, M. R.; Membrane chromatography-an integrative concept in the downstream processing of proteins. *Biotechnol. Prog.* **1995**, *11*, 357–367.
4. Min, M.; Shen, L.; Hong, G.; Zhu, M.; Zhang, Y.; Wang, X., Micro-nano structure poly(ether sulfones)/poly(ethyleneimine) nanofibrous affinity membrane for adsorption of anionic dyes and heavy metals ions in aqueous solution. *Chem. Eng. J.* **2012**, *197*, 88-100.
5. Ma, H.; Burger, C.; Hsiao, B. S.; Chu, B., Ultra-fine cellulose nanofibers: new nano-scale materials for water purification, *J. Mat. Chem.* **2011**, *21*, 7507-7510.
6. Ma, H.; Burher, C.; Hsiao, B. S.; Chu, B., Nanofibrous Microfiltration membrane based on cellulose nanowhiskers. *Biomacromolecules* **2012**, *13*, 180-186.
7. Karim, Z.; Mathew, A. P.; Grahn, A.; Mouzon, J.; Oksman, K., Nanoporous membranes with cellulose nanocrystals as functional entity in chitosan: Removal of dyes from water. *Carb. Poly.* **2014**, *112*, 668-676
8. Henriksson. M.; Berglund L.A.; Isaksson, P.; Lindstrom, T.; Takashi Nishino, T.; Cellulose Nanopaper Structures of High Toughness, *Biomacromolecules*, **2008**, *9*, 1579-1585.
9. Sehaqui, H.; Zhou, Q.; Ikkala, O.; Berglund, L. A., Strong and tough cellulose nanopaper with high specific surface area and porosity. *Biomacromolecules* **2011**, *12*, 3638-3644.
10. Mathew, A. P.; Oksman, K.; Karim, Z.; Liu, P.; Khan, S. A.; Naseri, N., Process scale up and characterization of wood cellulose nanocrystals hydrolyzed using bioethanol pilot plant. *Indus. Crop Prod.* **2014**, *58*, 212-219.
11. Bozic, M.; Peng, L.; Aji, P. M.; Kokol, V., Enzymatic phosphorylation of cellulose nanofibers to new highly-ions adsorbing, flame-retardant and hydroxyapatite-growth induced natural nanoparticles. *Cellulose* **2014**, *21*, 2713-2726..

12. Liu, P.; Sehaqui, H.; Tingaut, P.; Wichser, A.; Oksman, K.; Mathew, A. P., Cellulose and chitin nanomaterials for capturing silver ions (Ag⁺) from water via surface adsorption. *Cellulose* **2014a**, *21*, 449-461.
13. De-Mesquita, J.; Donnici, C. L.; Pereira, F. V., Biobased nanocomposite from layer-by-layer assembly of cellulose nanowhiskers with chitosan. *Biomacromolecules* **2010**, *11*, 473-480.
14. Visvanathan, C.; Aim, B. R.; Parameshwaran, K., Membrane separation bioreactor for wastewater. *Crit. Rev. Environ. Sci. Technol.* **2000**, *30*, 1-48.
15. Liu, P.; Ferrer, P.; Oksman, K.; Bozic, M.; Kokol, V.; Mathew, A. P., Nanocellulose for selective surface adsorption of Ag⁺, Cu²⁺ and Fe³⁺ from water Effective modification and metal ion concentration. *J. Hazar. Mater* **2014**. (communicated)
16. Takeshi, F.; Matsushima, K.; Kikuchi, K. I., Preparation of alginate chitosan hybrid gel beads and adsorption of divalent metal ions. *Chemosphere* **2014**, *55*, 135-140.
17. Lu, H.; Gui, Y.; Zheng L.; Liu, X., Morphology, crystallinity, thermal and physiochemical properties of cellulose nanocrystals obtained from sweet potato residue. *Food Res. Int.* **2013**, *50*, 121-128.
18. Liu, D.; Ti, Z.; Zehui, L.; Donglin, T.; Lie, C., Chitin nanofibers for rapid and effective removal of metal ions from waster system. *Carbohydrate Poly.* **2013**, *98*, 483-489.
19. Monreno, J.; Gomez, C.; Rigoberto., L.; Giraldo, L., Removal of Mn, Fe, Ni and Cu ions from wastewater using cow bone charcoal. *Materials* **2010**, *2*, 452-466.
20. Herrera, I.; Gardea-Torresdey, J. L.; Tiemann, K. J.; Peralta-Videa, J. R.; Armendariz, V.; Parsons, J. G., Binding of silver (I) by alfalfa biomass (*Medicago sativa*): Batch pH. time, temperature and ionic strength studies. *J. Hazard. Subs. Res.* **2003**, *4*, 1-15.
21. Theresa, A.; Dankovich, G.; Gray, D. G., Bacterial paper impregnated with silver nanoparticles for point-of-use water treatment. *Environ. Sci. Technol.* **2011**, *45*, 1992-1998.
22. WHO: Guidelines for drinking water quality. 3rd Edn., Vol 1Recommendations, Geneva, Switzerland (**2004**).
23. Lai, C. H.; Lo, S. L.; Chiang, H. L., Adsoption/desoptioin properties of copper ions on the surface of iron-coated sand using BET and EDAX. *Chemosphere* **2000**, *41*, 1249-1255.

24. Gadhave, A., Waghmare, J. Removal of heavy metal ions from wastewater by carbon nanotube (CNTs). *Inter. J. Chem. Sci. Appl.* 2014; 5: 56-67.

